Stability Analysis of a Turbocharger for Marine Diesel Engine Service

by

Michael S. Adams

Thesis submitted to the Faculty of the Virginia Polytechnic Institute and State University
in partial fulfillment of the requirements for the degree of

Master of Science
in
Mechanical Engineering

R. Gordon Kirk, Chair
Mary E. Kasarda
Alan A. Kornhauser

April 25, 2012
Blacksburg, Virginia

Keywords: turbocharger, stability, fluid-film bearings, rotordynamics

Stability Analysis of a Turbocharger for Marine Diesel Engine Service

Michael S. Adams

ABSTRACT

Rotor stability is essential to the life span of any piece of rotating machinery; it becomes increasingly critical in high-speed machinery such as turbochargers. Large turbochargers, such as those found in marine diesel propulsion engines where the rotor alone often exceeds forty pounds, require careful consideration regarding stability as well as load support during the bearing selection process. Logarithmic Decrement is the primary consideration for rotor stability. Commercial software is used to model and analyze a proven unstable turbocharger rotor. After confirming that the model exhibits unstable characteristics, the same turbocharger is then analyzed with various fluid-film bearing configurations. Finally, the tilting-pad bearing is determined to be the best bearing for this turbocharger application, stabilizing the rotor throughout the entire designed operating range.

Acknowledgments

First and foremost, I must thank the U.S. Coast Guard for supporting me with the time and funding necessary to further my education and work towards my Master's Degree. Without its support this opportunity would never have been possible.

I greatly appreciate, and am indebted to the support and encouragement from my family and colleagues while adapting back to an academic setting after five years of work in the fleet; they certainly helped keep my feet on the ground when the challenges arose.

To Dr. Kirk, Dr. Kasarda, and Dr. Kornhauser I am grateful for the support and guidance they provided not only with research, but my academic experience as a whole.

Finally, I would like to thank the administrative personnel, especially Cathy Hill, for providing guidance ensuring that I met all of my graduation requirements.

Table of Contents

LIST OF FIGURES

List of Tables

NOMENCLATURE

m	Mass or Preload of bearing
α	Offset of bearing
C_b	Bearing minimum assembled radial clearance
C_p	Pad machined radial clearance
r_p	Pad machined radius
r_j, r_s	Shaft or Journal radius
r_b	Bearing radius
e	Eccintricity of journal (distance between centers of bearing and journal)
O_b	Geometric center of bearing
O_j	Geometric center of journal
O_p	Pad center of curvature
θ_{pi}	Angle of center of curvature of lobe (pad i)
θ_{1i}	Angle of leading edge of lobe (pad i)
θ_{2i}	Angle of trailing edge of lobe (pad i)
D	Diameter (used for bearing surface, ring inner/outer surface, etc)
L	Bearing axial length
N	Rotor speed (RPM)
N’	Rotor speed (Revolutions per second)

CHAPTER 1

Introduction and Literature Review

1.1 *Introduction*

This thesis will present recent failures of turbo chargers in use on the main propulsion engines onboard sea-going buoy tenders, discuss analytical modes of failure, and conclude with a bearing modification which will provide improved turbocharger stability. This fleet of vessels, produced with a price tag of nearly $40 million each, is made up of sixteen ships separated into two classes. Five A-class vessels were placed into service prior to year 2000 and 11 B-class vessels after 2001. The vessels are propelled by Caterpillar 3608 engines which are similar in both classes. A significant difference between the two classes is the turbochargers used on the vessels. The A –class vessels utilize ABB VTC 254 turbochargers and the B-class utilizes Napier NA 297 turbochargers. The turbochargers were changed to accommodate changes in emissions regulations issued by the International Maritime Organization. To date, the A-class vessels have experienced in excess of twenty turbocharger failures, while the B-class has experienced only 1 failure. Most of the failures have demonstrated evidence of shaft shear, bearing damage, and in some cases contact of the compressor with the turbocharger housing. Each turbocharger costs nearly sixty-thousand dollars to replace in whole, and nearly $30,000 if only the rotating assembly is in need of replacement. In the sections to follow, the method of failure will be reviewed as well as the potential contributing causes of failure, and recommendations will be made for future consideration. The assumptions are made that the turbochargers are both appropriate for the given application, and that neither the engine application nor foreign object debris are causative factors in the turbocharger failure.

The use of bearings to simplify the movement of objects has been confirmed as early as 40 BC and is speculated to have taken place thousands of years before. Since wooden balls were used to create simple turn-tables nearly two thousand years ago aboard Roman ships, the design, application, and in most cases complexity of bearings has grown immensely [1]. The global bearing industry has been valued to over $40 billion annually and remains a focus of research efforts [2]. Since the focus of this paper is on bearing application in turbochargers, the fluid-film bearing will be of primary focus. As opposed to the rolling element bearing where the load is supported by a series of encaged rolling balls, cylinders, or needles, fluid-film bearings rely on an oil film generated between the rotating and stationary elements of the system. This oil film is the only barrier against metal to metal contact, self-excited instabilities, and ultimately failure of the bearing. In most cases, these bearings are hydro-dynamic, where the viscous properties of the lubricating oil combined with the differential in relative speed, and the converging clearance, between the journal and bearing surfaces are responsible for the generation of the pressure profile of the fluid film [3]. In some cases the bearings may be hydro-static in nature, where an external pump supplies lubricating oil at a specified pressure to establish a fluid film prior to the start up of the machine. This method of oil delivery is typically only found in situations involving heavily loaded bearings and low viscosity and/or low linear velocity applications [4]. The fluid-film bearings in use today can be separated into two main categories, and further broken down thereafter. The two main categories are fixed-geometry, where the bearing does not change shape while in use, and non-fixed geometry where the bearing is designed to conform to dynamic operating conditions. Fixed-geometry bearings typically consist of plain journal bearings, axial groove bearings, and multi-lobe bearings, while non-fixed geometry bearings commonly consist of tilting-pad bearings and floating ring bearings. All bearings have specific

strengths and weaknesses; knowledge and experience is required to properly select bearings for specific applications. The most significant considerations for proper bearing selection are cost, manufacturability and ease of installation and replacement, static performance, and dynamic performance. Static performance considerations include film thickness and pressure gradients in fluid-film bearings, power loss, and operating temperature while dynamic considerations include synchronous and sub-synchronous vibrations, critical speeds, and system stability [3].

1.2 *Literature Review*

For nearly a century the concept of forced induction including superchargers and turbochargers has been investigated with application to the internal combustion engine. The specific concept of turbo charging involves a turbine powered by the engine's exhaust gases, often reaching speeds exceeding 100,000 rpm, which is rigidly connected to a compressor that forces the incoming air to above ambient pressure in the engine's intake. Watson et al. [5] explores forced induction and its impact on the power generated from an internal combustion engine compared to a naturally aspirated engine of similar size. In current times where more power is needed in smaller spaces, the reliance on turbochargers has greatly increased. As the performance threshold of turbochargers is pushed, various problems have risen, including the issue of rotor-bearing system stability. Instabilities in rotors are often quantified using logarithmic decrement. Logarithmic decrement is further defined in Chapter 3, and in its most simple form is the ratio of successive vibration amplitudes. A simple shaft spinning at a high enough speed can encounter self-generated, sub-synchronous instabilities; the situation is worsened when the shaft, supported from the center, has a loaded rotor at each end (known as "double overhung"), as is visible in the model shown in Figure 1.1 [3]. This instability can be mitigated via one of two methods. Method one is to redesign the entire rotor system and analyze

the system with commercial software, making incremental changes until instabilities are corrected. The second method is to consider the instabilities and, if possible, install a bearing capable of reducing or eliminating those instabilities. Both of these methods require analysis to define the source of instability, followed by a re-design of a specific component to restore stability. Cost is typically the determining factor in accounting for instabilities. For high cost equipment produced in low quantities, the higher cost bearings may prove appropriate. On the other hand, an automotive turbocharger could nearly double in cost if, for example, tilting pad bearings, which are commonly quite expensive, are installed in place of plain journal bearings, which are the most inexpensive of all fluid-film bearing types. In this case, it becomes appropriate to consider design modifications to restore stability and maintain a relatively low cost of production.

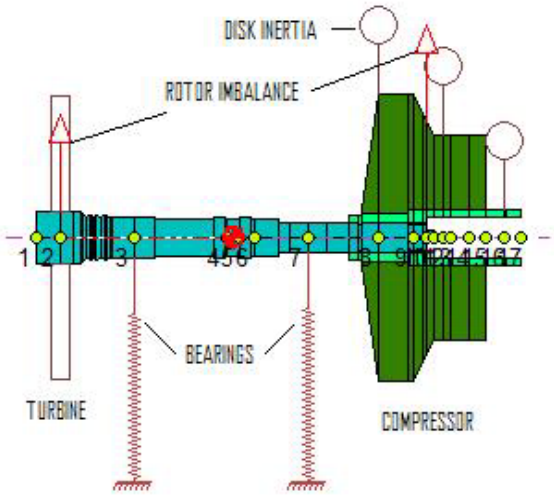

Figure 1.1: DyRoBeS generated model of ABB turbocharger rotor.

Turbocharger vibration has been shown to be the result of forces caused by rotor and/or shaft unbalances, self-excited forces, or in many cases a combination of both. While unbalance forces typically stem from shaft eccentricities or bows and can usually be identified and corrected with relative ease prior to bringing a turbocharger up to speed, self-excited instabilities

are non-existent until the rotor is spinning. Alsaeed [6] discusses the challenges that were historically present in predicting these instabilities prior to experimentation, and recognizes the software advances which have taken place, allowing for the fast and accurate analytical analysis of rotor-bearing systems. Ehrich [7] attributes most self-excited instabilities to whipping and whirling, parametric instabilities, stick-slip rubs and chatter, and forced vibrations induced through foundations by nearby machinery. Whipping and whirling typically result from the viscous fluid (lubricating oil) traveling in fluid-film bearings with a velocity of approximately one-half that of the surface of the rotating shaft. In many cases this oil is the primary cause of strong sub-synchronous vibrations which can have devastating results, especially at rotor speeds of approximately twice that of the first critical. In other cases, excitation of natural frequencies occurring from the dynamics of the rotor itself can be a design burden. Computer programs can accurately model system instabilities during the design process, making it possible for manufacturers to have confidence that a stable piece of machinery will be produced prior to the first piece being cut. These software tools, such as DyRoBeS (Dynamics of Rotor Bearing Systems) Rotor [8] and DyRoBes BePerf (Bearing Performance) [9] have greatly improved the quality of products, while decreasing the associated cost of design and testing [10]. Many texts discuss the specific sources of instabilities in great detail, thus it is not the focus of this paper to reproduce those findings. DyRoBeS will be the software used to produce theoretical results related to the failure of the turbocharger in question, and bearing modifications will be the focus for restoring stability in the system.

To counter the instabilities of a rotor-bearing system, modifications ranging from the type of bearings used to the geometry of the bearing, preloads, oil viscosity, etc can be implemented. Because turbochargers routinely use the same oil as the engine which they serve, it is often

difficult to change the oil viscosity, so other means must be used to stabilize an otherwise unstable system. To avoid the cost of completely re-designing the turbocharger, bearing selection is often the area of focus for stabilization. Simply changing the geometry of a floating ring bearing may require little to no alteration to the bearing housing, while changing the bearing type (i.e. from a floating ring to a tilting pad) will require substantial machine work. Software can be used to model the system prior to and after these modifications, and the initial and new stability studied, again before any experimentation ever takes place [10]. Bearing selection becomes critical in the design process of the rotor-bearing system, as some bearings provide high load carrying capability with low levels of damping, while others provide substantial damping but are susceptible to failure upon exposure to high load situations. Conditions requiring high levels of both damping and stiffness will likely result in the need for a higher cost bearing, such as the multi-lobe or tilting-pad bearing. Damping and stiffness graphs for specific bearings are available from many bearing manufacturers, and can also be generated by software programs. These damping and stiffness graphs are often a function of the *Sommerfeld Number,* which is dimensionless in nature and can be calculated in multiple ways; an example of these graphs can be seen in Figure 1.2. The most common form of the Sommerfeld Number (S) is given by equation (1.1):

$$S = \frac{\mu N' L D}{W}\left(\frac{R}{c}\right)^2 \tag{1.1}$$

where μ viscosity in reyns
N' shaft rotational speed (Rev/sec)
L axial length of the bearing pad (inches)
D pad length (inches)
W bearing load (pounds, lbf)
R journal radius (inches)
c pad-bore radial clearance (inches) [4]

Note, in some cases, authors will combine some terms to yield:

$$S = \frac{\mu N'}{P}\left(\frac{R}{c}\right)^2 \tag{1.1b}$$

In this case, the load, length terms, and the bearing load have been combined to form a force per unit area term in the denominator. It is unique that the rotor speed, in this equation, is expressed in terms of revolutions per second, rather than the typical revolutions per minute.

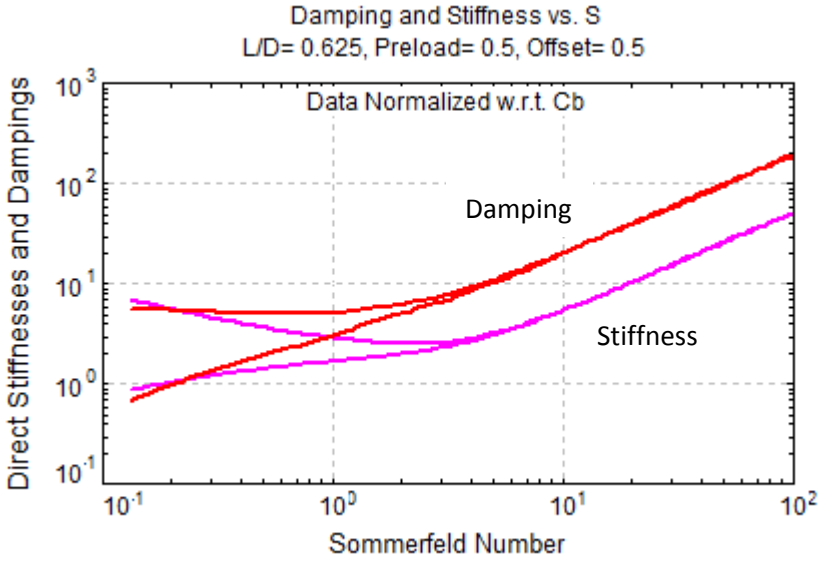

Figure 1.2: Stiffness (pink) and Damping (red) vs. Sommerfeld Number.

Especially prevalent in the automotive market, where small high speed turbochargers are most common, floating-ring journal bearings provide a significant amount of stiffness and damping to a system at a fraction of the cost of other bearings. While floating-ring bearings, such as that illustrated in Section 1.4, are useful in high speed, low load applications, their relatively low cost comes with a risk. Because they rely on tight clearances to generate the higher pressures needed to support loads, these bearings are susceptible to failure in applications where an increased load or vibration may be encountered, causing the journal to come into contact with the floating bush, or the floating bush with the outer bearing surface [4]. While

metal to metal contact is encountered at every start up until a hydrodynamic fluid film is established, contact at operating speed can cause serious damage to the bearing surface and result in bearing failure [10]. Bearing failure may, in some cases, be detected before catastrophic failure of the entire piece of machinery; however, in many cases a failed bearing will seize to the shaft. A floating bush which seizes to the journal while at operating speeds will exhibit similar characteristics as a plain journal bearing with excessive clearances leading to high whirling amplitudes, which may allow for contact between the turbine or compressor blades with the turbocharger housing. The damage and debris contamination caused by rotor contact will typically render the entire unit unserviceable [11].

Rolling element bearings, although not a fluid-film bearing, have been applied to high speed applications with relatively little success. Their relatively short lifespan renders them useful only in limited specialty applications, such as automotive racing, where the time and cost involved in frequent maintenance is not prohibitive [10]. This is not the case for large industrial engines, and is not applicable to this discussion.

1.3 *Reynolds Equation Derived*

A bearing's ability to support a load is a function of several characteristics, all of which affect the flow of the fluid film. The bearing style and geometry, operating speed, and oil viscosity all contribute to the bearing's ability to support a load and dampen vibration. The Reynolds Equation is the foundation of most calculations regarding fluid flow through the bearing and thus the resulting damping and stiffness characteristics. In the lines that follow, the x-axis is defined in the direction of relative motion, the y-axis will be defined in the direction of the bearing clearance, and the z-direction is defined in the direction of the length of the bearing.

The Reynolds Equation can be derived from the Navier-Stokes and Continuity Equations, assuming constant viscosity and density, as follows:

Navier-Stokes:
$$\rho\frac{D\bar{v}}{Dt} = \bar{B}\rho - \bar{\nabla}\rho + \mu\left[\frac{1}{3}\bar{\nabla}(\bar{\nabla}\cdot\bar{v}) + \nabla^2\bar{v}\right] \tag{1.2}$$

Continuity:
$$\frac{\partial\rho}{\partial t} + \frac{\partial(\rho u)}{\partial x} + \frac{\partial(\rho v)}{\partial y} + \frac{\partial(\rho w)}{\partial z} = 0 \tag{1.3a}$$

Or, in tensor notation:
$$\frac{D\rho}{Dt} + \rho(\bar{v}\cdot\bar{\nabla}) = 0 \tag{1.3b}$$

Assuming that body forces ($\bar{B}$) and inertial forces ($\frac{D\bar{v}}{Dt}$) are non-existent, the pressure gradient in the y-direction is zero, and that the fluid flow is laminar in nature, the Navier-Stokes equations become:

$$0 = -\frac{\partial P}{\partial x} + \mu\frac{\partial^2 u}{\partial y^2} \tag{1.4a}$$

$$0 = -\frac{\partial P}{\partial z} + \mu\frac{\partial^2 w}{\partial y^2} \tag{1.4b}$$

Equation (1.4a) can be modified and integrated twice with respect to y to become:

$$u(y) = \frac{1}{2\mu}\frac{\partial P}{\partial x}y^2 + C_1 y + C_2 \tag{1.5}$$

Boundary conditions can now be considered:

At y=0:
$$u = U_1 \therefore C_2 = U_1 \tag{1.6}$$

And at y=h:
$$u = U_2 \tag{1.7}$$

Inserting equation (1.7) into equation (1.5), and solving for C_1 yields:

$$C_1 = \frac{U_2 - U_1}{h} - \frac{h}{2\mu}\frac{\partial P}{\partial x} \tag{1.8}$$

Inserting equation (1.8) into equation (1.5) the velocity equation becomes:

$$u(y) = \frac{1}{2\mu}\frac{\partial P}{\partial x}(y^2 - yh) + \frac{h-y}{h}U_1 + \frac{y}{h}U_2 \tag{1.9}$$

Similarly, the equation for velocity in the z-direction can be shown to become

$$w(y) = \frac{1}{2\mu}\frac{\partial P}{\partial z}(y^2 - yh) + \frac{h-y}{h}W_1 + \frac{y}{h}W_2 \tag{1.10}$$

Integrating and rearranging the Continuity equation:

$$\int_0^h \frac{\partial(\rho v)}{\partial y}dy = -\left\{\int_0^h \frac{\partial \rho}{\partial t}dy + \int_0^h \frac{\partial \rho u}{\partial x}dy + \int_0^h \frac{\partial \rho w}{\partial z}dy\right\} \tag{1.11}$$

Applying Leibniz's rule for differentiation under an integral yields the velocity equations (x and z direction, respectively):

u:
$$\int_0^h \frac{\partial \rho u}{\partial x}dy = -\frac{\partial}{\partial x}\left[\frac{\rho h^3}{12\mu}\frac{\partial p}{\partial x}\right] + \frac{\partial}{\partial x}\left[\frac{1}{2}\rho h(U_1 + U_2)\right] - \rho U_2\frac{\partial h}{\partial x} \tag{1.12a}$$

w:
$$\int_0^h \frac{\partial \rho w}{\partial z}dy = -\frac{\partial}{\partial z}\left[\frac{\rho h^3}{12\mu}\frac{\partial p}{\partial z}\right] + \frac{\partial}{\partial z}\left[\frac{1}{2}\rho h(W_1 + W_2)\right] - \rho W_2\frac{\partial h}{\partial z} \tag{1.12b}$$

Applying equations (1.12a) and (1.12b) to equation (1.11) and integrating yields the equation:

$$\begin{aligned}\rho(V_2 - V_1) = &-\frac{\partial \rho}{\partial t}h + \frac{\partial}{\partial x}\left[\frac{\rho h^3}{12\mu}\frac{\partial P}{\partial x}\right] - \frac{\partial}{\partial x}\left[\frac{1}{2}\rho h(U_1 + U_2)\right] + \rho U_2\frac{\partial h}{\partial x} \\ &+ \frac{\partial}{\partial z}\left[\frac{\rho h^3}{12\mu}\frac{\partial P}{\partial z}\right] - \frac{\partial}{\partial z}\left[\frac{1}{2}\rho h(W_1 + W_2)\right] + \rho W_2\frac{\partial h}{\partial z}\end{aligned} \tag{1.13}$$

This equation can be simplified by multiplying by 12, letting $V = V_2 - V_1$, $W_2 = W_1 = 0$, and $\frac{\partial h}{\partial z} = 0$, and after rearranging becomes:

$$\frac{\partial}{\partial x}\left[\frac{\rho h^3}{\mu}\frac{\partial P}{\partial x}\right]+\frac{\partial}{\partial z}\left[\frac{\rho h^3}{\mu}\frac{\partial P}{\partial z}\right] = 12\rho V + 12h\frac{\partial \rho}{\partial t} + 6\frac{\partial}{\partial x}[\rho h(U_1 - U_2)] - 12\rho U_2\frac{\partial h}{\partial x} \tag{1.14}$$

Applying the incompressible assumption and setting $V = \frac{\partial h}{\partial t}$, equation (1.14) reduces to the more common known Reynolds Equation:

$$\frac{\partial}{\partial x}\left[\frac{h^3}{\mu}\frac{\partial P}{\partial x}\right]+\frac{\partial}{\partial z}\left[\frac{h^3}{\mu}\frac{\partial P}{\partial z}\right] = 12\frac{\partial h}{\partial t} + 6(U_1 - U_2)\frac{\partial h}{\partial x} + 6h\frac{\partial}{\partial x}(U_1 + U_2) \tag{1.15}$$

Because the geometry of bearings varies greatly, linear velocity is typically used rather than rotational velocity when discussing load handling capabilities of a bearing. Linear velocity is simply a function of radius and rotational velocity, and forms the values for variables $U_1$and U_2 used above. Equation (1.15) is the most general form of the Reynolds Equation, applicable to slider bearings. Kirk and Gunter [12] continue the Reynolds Equation making additional assumptions to arrive at the form of the Reynolds Equation applicable to journal bearings, shown in equation (1.16).

$$\frac{1}{6}\left[\frac{1}{R^2}\frac{\partial}{\partial \theta'}\left(\frac{h^3}{\mu}\frac{\partial P}{\partial \theta'}\right)+\frac{\partial}{\partial z}\left(\frac{h^3}{\mu}\frac{\partial P}{\partial z}\right)\right] = \left(\omega_b + \omega_j - 2\dot{\Phi}\right)\frac{\partial h}{\partial \theta'} + 2\frac{\partial h}{\partial t} \tag{1.16}$$

The Reynolds Equation still reduces to a series of equations dependent on time and position; it becomes obvious that FEA software is so valuable in this study.

1.4 *Bearing Review*

The more specific bearing types and their characteristics are presented below, with figures developed using the DyRoBeS BePerf program [9]. The second figure of each bearing type presents a basic pressure profile to make more visible the principles of operation of the

bearing. A few concepts of bearing theory must be discussed before presenting the various bearing types. Fluid-film bearings consist of a pad or series of pads located around the outer diameter of the rotating shaft, or journal. The concept of "Preload" involves the use of bearing pads with a radius greater than that of the journal. Preloading allows the center of curvature of the pad to be moved closer to the journal, creating a higher pressure. The preload of a bearing is often defined by the variable m and is defined by equation (1.16):

$$m = \frac{C_p - C_b}{C_p} = 1 - \frac{C_b}{C_p} \tag{1.16}$$

Where: $C_b = r_b - r_s$ and $C_p = r_p - r_s$

A value of zero would indicate no preload, that is, the shaft is centered in the bearing, while a value of 1 would indicate no clearance between the shaft and bearing, or each pad [13]. In cases where preload exists and reverse rotation of the shaft is not a possibility, the pads may be offset, also known as "lobe tilt," which is the ratio of converging pad surface compared to the total arc length, and is defined by the variable α. An offset of 0.5 indicates no offset; a value of less than 0.5 would create a diverging surface and have a similar effect as a reversed-rotation shaft creating instabilities, and is thus undesirable. The offset value is calculated by dividing the arc length of the pad's converging surface by the total arc length of the pad using equation (1.17) [9]:

$$\alpha = \frac{\theta_p - \theta_1}{\theta_2 - \theta_1} \tag{1.17}$$

Fixed Geometry:

Plain Journal- The plain journal bearing is the most basic of fluid-film bearings, shown in Figure 1.3, and involves a shaft which spins within the circumference of a single, continuous outer

bearing surface, suspended by a thin film of lubricating oil. The simplicity of this bearing type renders it relatively inexpensive; however, the low cost comes at the price of high destabilizing forces. The continuous, uninterrupted fluid film undergoes whirling creating cross-coupled forces, which continue to grow with increased speeds. In addition to high cross-couple forces, the plain journal bearing has relatively low damping compared to other options, leaving it susceptible to self-excited rotor instabilities [4].

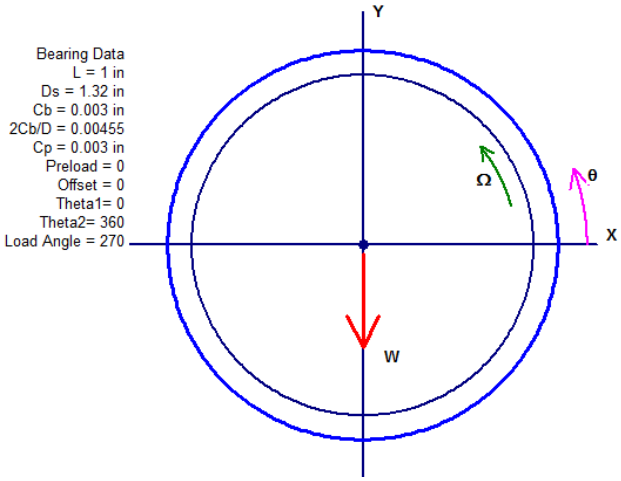

Figure 1.3a: Typical Plain Journal bearing cross section.

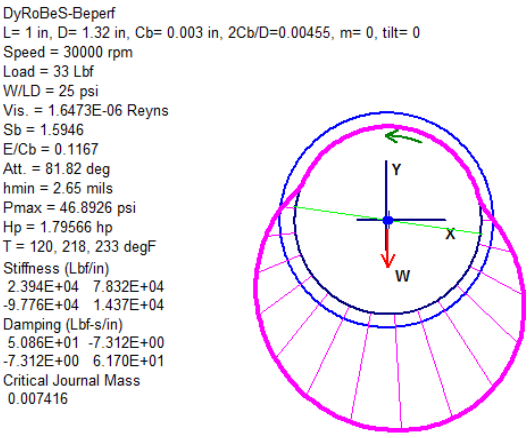

Figure 1.3b: Typical Plain Journal bearing pressure profile.

Axial Groove-Although similar to the plain journal bearing, the axial groove bearing differs in that it has length-wise grooves cut in the outer bearing surface, parallel to the axial length of the journal, seen in Figure 1.4. These grooves allow for greater oil supply, which helps to reduce (but not eliminate) the self-induced instabilities found in the plain journal bearing. The cost of the axial groove bearing is slightly higher than that of the plain journal bearing due to the added machining required to create the grooves [4].

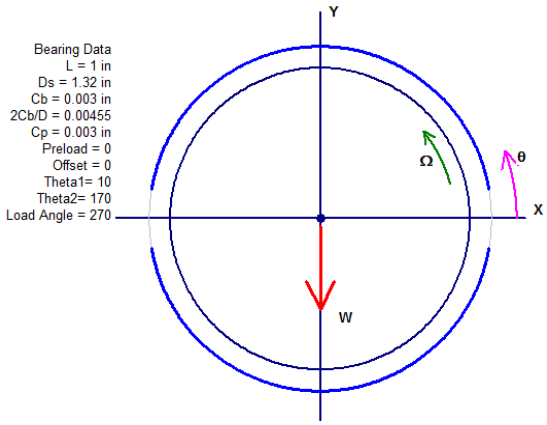

Figure 1.4a: Typical Axial Groove bearing cross section.

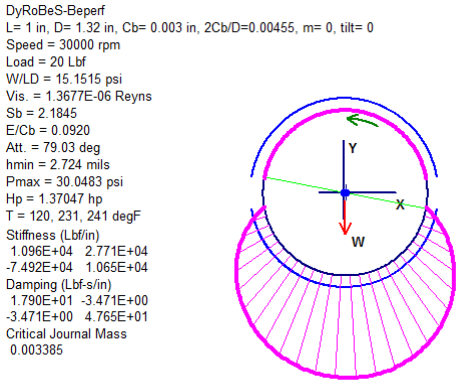

Figure 1.4b: Typical Axial Groove bearing pressure profile.

Elliptical- The elliptical or lemon-bore bearing, seen in Figure 1.5, has a lemon-shaped profile, that is, the bore of the bearing is oblong with grooves machined at the ends of the bore. Oil is supplied in the grooves and is picked up by the rotating shaft. The converging clearance between shaft and bearing creates a pressure gradient which tends to somewhat reduce shaft instabilities such as whirl, but still introduces cross-coupling instabilities. The elliptical bearing is still relatively inexpensive, but more costly than the axial groove bearing [4].

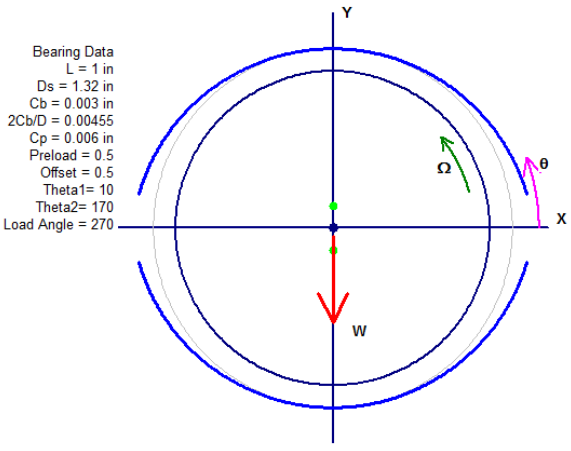

Figure 1.5a: Typical Elliptical (or Lemon-bore) bearing cross section.

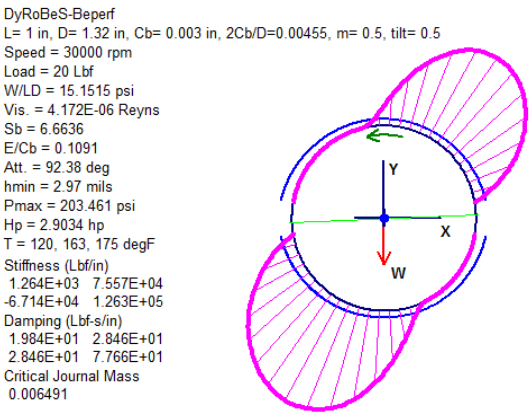

Figure 1.5b: Typical Elliptical bearing pressure profile.

Offset Half- The offset half bearing is similar to an elliptical journal bearing, cut in half (upper and lower, for example). The halves are staggered, as seen in Figure 1.6, by approximately half the clearance radius. Similar to the elliptical bearing, this creates a pressure gradient which reduces the whirl of the shaft; although, cross-coupling is still present as a result of the bearing. The improved stability comes at an additional cost in that the stagger (offset) of the halves yields the bearing effective in only one direction of motion, and the converging surfaces do result in power losses [4].

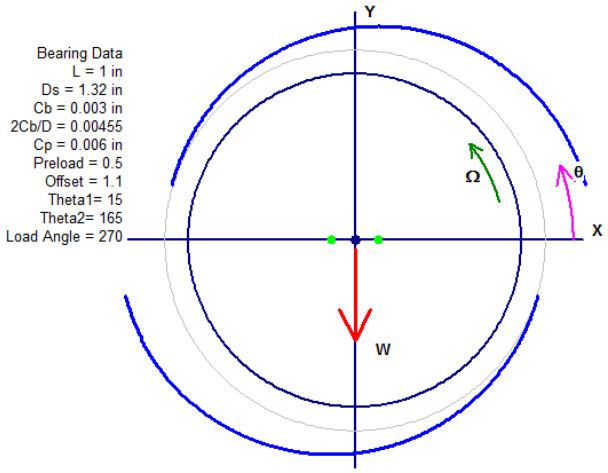

Figure 1.6a: Typical Offset Half bearing cross section.

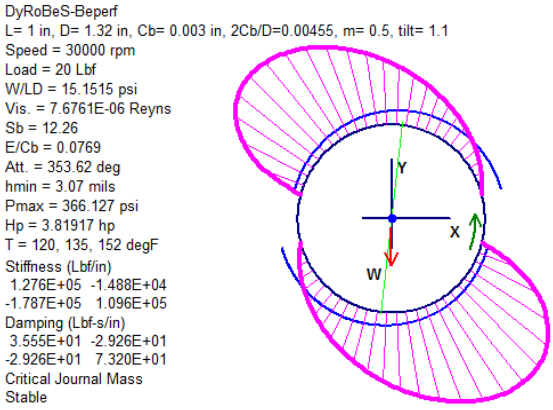

Figure 1.6b: Typical Offset Half bearing pressure profile.

Multi-lobe- The outer surface of multi-lobe bearing is made up of a series of individual segments ("lobes" or "pads") separated by axial grooves which provide an oil supply to the bearing as seen in Figure 1.7, similar to the axial groove bearing. This scheme generates a series of converging surfaces, creating pressure gradients as are visible in Figure 1.7b; note that the more heavily loaded lobes, where clearances become tighter, create higher pressures, as expected. While this concept provides a greatly improved damping (stabilizing) effect over plain journal bearings, it

comes at a higher manufacturing cost, as well as the robbing of power from the system in which it serves due to the multiple converging surfaces.

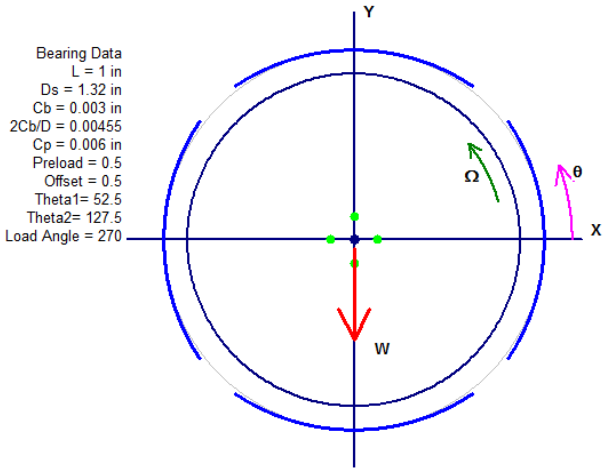

Figure 1.7a: Typical Multi-Lobe bearing cross section.

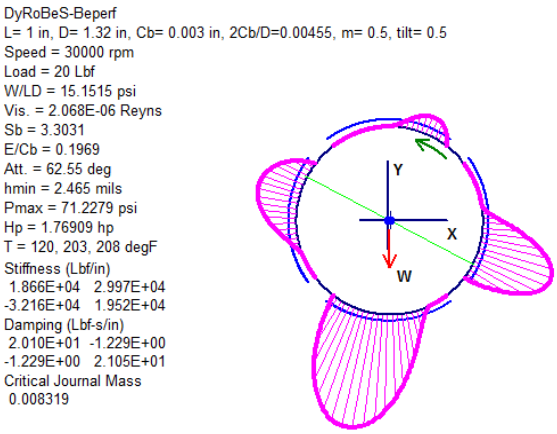

Figure 1.7b: Typical Multi-Lobe bearing pressure profile.

Pressure Dam- The pressure dam bearing is similar to an axial groove bearing with one key difference. A relief pocket is milled into the bearing surface, as seen in Figure 1.8. The relief begins gradually and ends abruptly; this sharp edge is the "dam" which results a pressure spike of the lubricating oil (hence "pressure dam"). This increased pressure, usually located on the top of the bearing, applies an artificial downward force on the shaft to greatly reduce instabilities. A relief is sometimes included over the entire radius of the loaded half of the bearing to increase the effects of the artificial loading of the pressure dam, further lessening instabilities induced by oil whirl. The artificial forces result in significant power losses, and the precise machining involved to fabricate this bearing is also significant. Additionally, this bearing is directional and thus a poor choice if the shaft could possibly reverse direction [3].

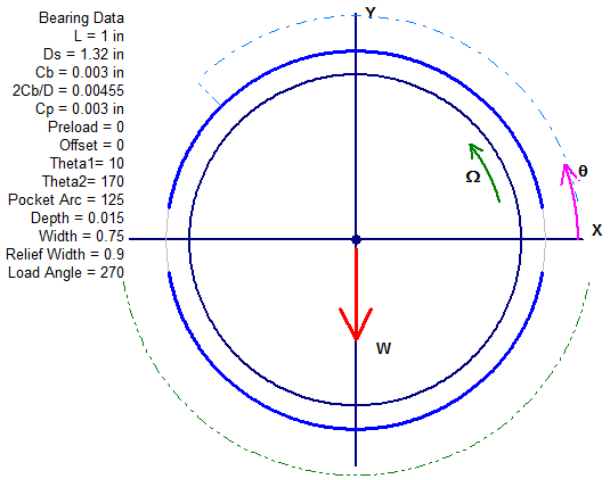

Figure 1.8a: Typical Pressure Dam bearing cross section.

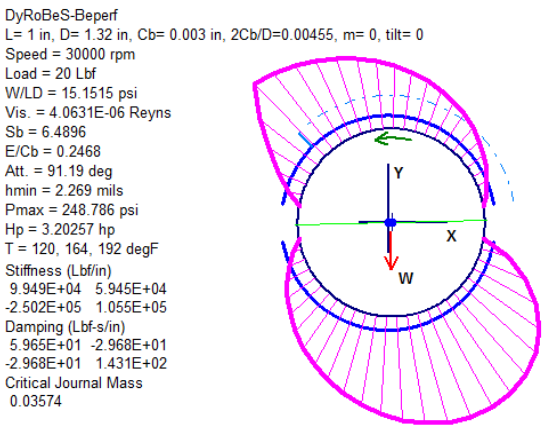

Figure 1.8b: Typical Pressure Dam bearing pressure profile.

Non-fixed geometry:

Floating-Ring Fluid-film- The floating ring (or floating bush) bearing has been developed for use in higher speed applications, and follows the same principles as the plain journal bearing. The floating ring bearing employs an intermediate ring between the journal (shaft) and outside bearing, separated from each by a thin oil film, seen in Figure 1.9. The intermediate ring is intended to rotate at approximately half the shaft speed, reducing the destabilizing cross-coupling forces that would otherwise be found in the plain journal bearing and generating a greater damping effect. The floating bush bearing is relatively inexpensive, and has significant loading limitations that will be discussed later in this paper [4].

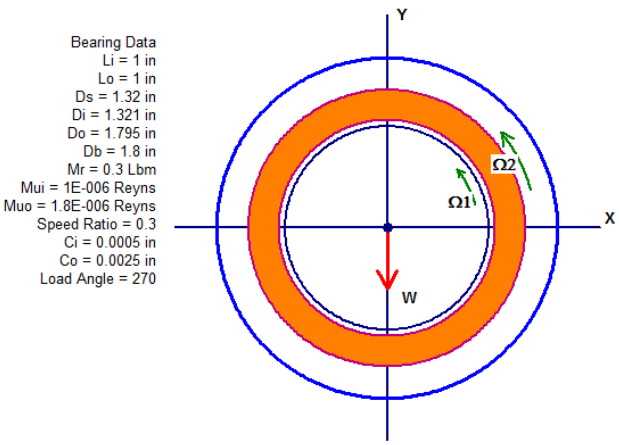

Figure 1.9a: Typical Floating-Ring bearing cross section.

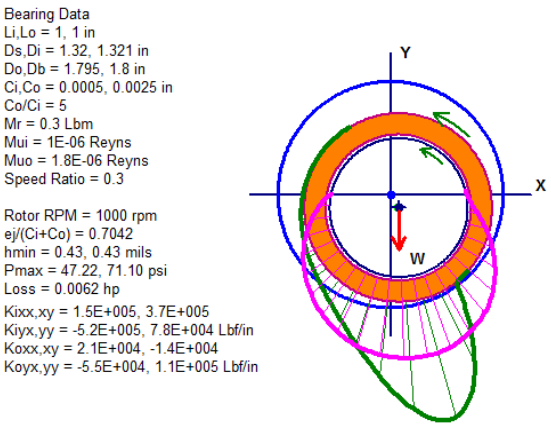

Figure 1.9b: Typical Floating-Ring bearing pressure profile. Note two fluid films exist, so two pressure profiles are generated.

Tilting Pad-Perhaps the most stable bearing design on the market today is the tilting pad bearing, visible in Figure 1.10. A series of pads (typically 3 to 5 pads) make up the bearing surface, which are free to pivot about a point or line on their back side. The radius of the pad is typically slightly larger than that of the rotating shaft, generating a preload, or converging wedge which creates a pressure gradient over its surface. The position of the pivot point with regard to the arced surface of the pad can be shifted to create an offset and increase the stabilizing effects and load capacity of the bearing; however, this shall only be done if there exists no possibility that the shaft can reverse rotation. When there exists no offset, the bearing is considered to be "centrally pivoted." While this bearing is extremely stable, there is a substantial financial cost involved due to the extensive precision machining involved in its fabrication as well as higher power losses while in operation than most bearing types due to the multiple converging surfaces. Additionally, this bearing leaves open the possibility of improper assembly, which has been known to take place in industry, with devastating results [4]. This bearing will be discussed in greater detail in chapter four.

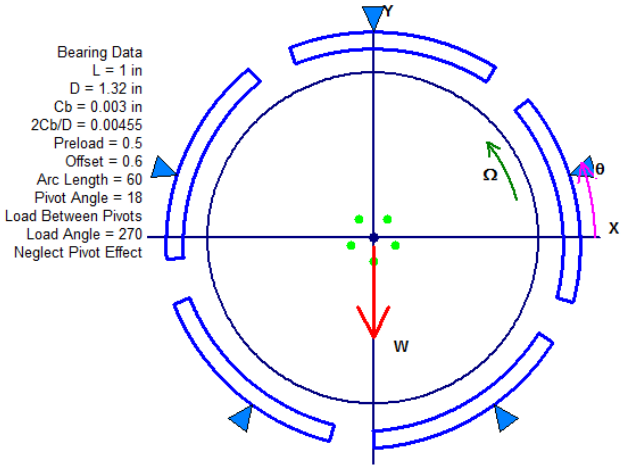

Figure 1.10a: Typical Tilting Pad bearing cross section.

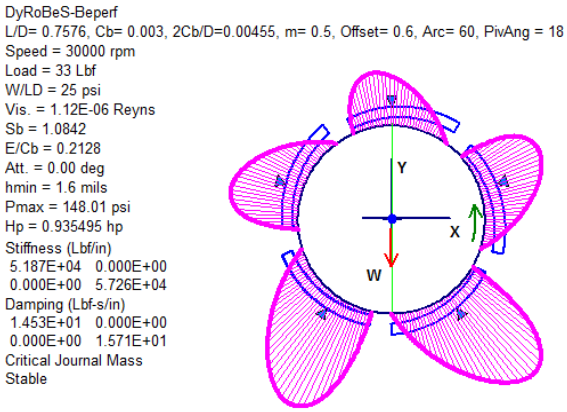

1.10b: Typical Tilting Pad bearing pressure profile.

One additional bearing that has become a major topic of research is in a class of its own, and is the magnetic bearing. Magnetic bearings can be considered as cutting edge technology in the world of bearings. Considerable fallbacks of magnetic bearings are their extreme cost, as they require a computer system to analyze shaft motion and adjust the bearing accordingly (upwards of $45k greater than a comparable fluid-film bearing) and their inability to function in an overload condition. While a fluid-film bearing can function for a finite time in an overload condition, it can be expected that a machine with overloaded magnetic bearings will suffer instantaneous failure [14]. Additionally, magnetic bearings require significantly more space than virtually all other bearings, eliminating their usage on turbochargers and other applications where conserving space is critical.

CHAPTER 2
MODEL DESIGN

2.1 *Model Considerations*

In most cases it is not practical to eliminate all of the instabilities, so accommodations must be made to minimize any negative impacts that they produce. While increasing bearing stiffness by reducing bearing clearance or adding preload may reduce sub-synchronous vibrations, increasing oil temperatures resulting from the tighter clearances will reduce oil viscosity reducing the bearing's load capacity. The accepted minimum bearing clearance for a journal bearings is approximately 1.5 mil per inch of journal diameter [4]. The risks of tight clearances are further amplified in cases where static loading conditions place the bearing near its mechanical limits before vibration is encountered. It becomes necessary to conduct a stability analysis to study the interaction of the rotor with the bearing, and ultimately the stability of the system as a whole prior to investing in funding to generate a working model. In this case, the turbocharger under analysis has already been generated and placed into service, and has proven to be unstable. The stability analysis will conclude with recommendations to restore stability.

To begin, the specific rotor was first modeled in DyRoBeS, due to the program's availability and ease of use; the modeled rotor is visible in Figure 1.9. This software is a series of two Finite Element Analysis based programs, one analyzing bearings and the other rotor-bearing systems. Once an accurate rotor model was generated, bearings were added to allow for the various simulations to be run, including determination of various torsional and lateral shaft vibrations, whirl speed, deflection, and bearing loading calculations. A key feature greatly simplifying the analysis of the turbocharger was the program's ability to export data files from

the bearing program to the rotor-bearing system program. Figure 2.1 identifies the various components of the rotor, further described in Table 2.1. While the owner of the turbocharger was unable to supply a unit to obtain direct measurements, a scaled drawing in addition to the shaft elements contained in Table 2.1 was provided. In order to model the rotor as accurately as possible, the inertias contained in Table 2.1 were used for the turbine disk and blades, thrust collar, compressor wheel and blades, and nosecone. DyRoBeS was used to calculate the inertias for the turbine shaft and impeller shaft, as accurate dimensions and material properties were known for these components.

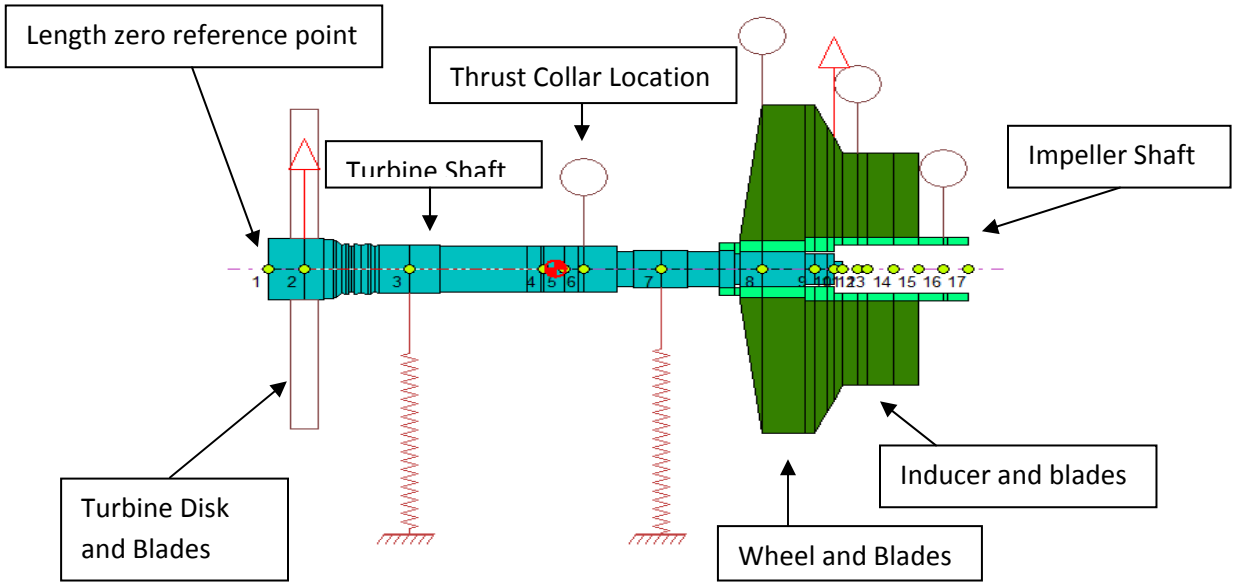

Figure 2.1: Location of Rotor Components

Table 2.1: Rotor component specifications

Component	Mass (lbm)	Axial Location ($in\ from\ turbine\ end$)	Polar Moment of Inertia ($lbm - in^2$)	Transverse Moment of Inertia ($lbm - in^2$)
Turbine Disk & Blades	15.7	1.02	146.2	74.6
Turbine Shaft	7.33	7.66	2.2	121.4
Thrust Collar	1.50	8.77	1.7	1.8
Wheel & Blades	9.51	13.70	111.5	58.3
Impeller Shaft	4.32	15.16	4.1	20.7
Inducer & Blades	4.19	16.34	25	15.8
Nosecone	0.48	18.86	0.68	0.43

2.2 *Generation of the Rotor Model*

The model was generated as a single steel shaft, with careful consideration taken to ensure dimensions are as close to the supplied drawing as possible. This allows for an accurate stiffness to be calculated by the program, which is critical to the accuracy of the stability analysis. Stiffness added by the thrust collar was neglected since the fit could not be analyzed. One analysis of this rotor has suggested that this collar had an excessive interference fit, upwards of eight mils, while other documents suggest an appropriate interference of approximately one mil. The added stiffness resulting from the thrust collar was neglected due to conflicting data. It is also noted that appropriate fit of the thrust collar is critical to prevent shaft bow. Due to the complex geometries of the turbine and compressor, the mass and inertias were placed at a point specified in Table 2.1. Bearing stiffness and damping data was added to the rotor model using output from DyRoBeS BePerf. DyRoBeS BePerf generated the bearing data using the dimensions shown in Table 2.3; this data follows industry standards since the actual unit was not provided for inspection. The existing bearing installed on this turbocharger is a hybrid of a

floating ring bearing. While the floating ring bearing is typical, the designer chose to modify the floating ring by cutting axial grooves in the inside radius. In theory, the axial grooves will increase the stiffness characteristics of the bearing, and maintain the damping characteristics of the floating ring bearing. This hybrid-style bearing is rare, and has some poor characteristics, as will be presented in the next chapter. While DyRoBeS is not designed to model such a bearing, it will be shown that some manipulations of current tools will allow for a reasonable approximation of this bearing design using the existing capabilities of DyRoBeS.

To rank the floating axial groove bearing among other bearings, a few bearing styles have been chosen for analytical implementation to this turbocharger. All rotor dimensions will be held constant, changing only the bearing characteristics (speed dependent stiffness and damping). The specific bearings considered for this analysis are the plain journal bearing, four axial groove bearing, and the 4 pad tilting pad bearing. When different bearings are analyzed, the turbine bearing will be of similar type as the compressor bearing, using similar dimensions for each bearing type. This selection of bearings will provide coverage of a broad spectrum of stiffness, damping, and cost; these relative characteristics are shown in Table 2.2 [15].

Table 2.2: Bearing Types and Relative General Characteristics

Bearing Type	Stiffness	Damping	Cost
Plain Journal	Low	Very High*	Low
4-Axial Groove	Moderate	Low	Moderate
4- Tilting Pad	High	High	High
Floating Axial Groove**	Unknown	Unknown	Moderate

*Although damping values are high, destabilizing cross-couple forces are typically dominant [4].
**Information for this bearing is to be determined, and is not discussed in reference [5].

Table 2.3a: Dimensions of Comparative Bearings, Compressor Side

Dimension	Plain Journal Bearing	4-Axial Groove Bearing	4-Tilting Pad Bearing	Floating Axial Groove Bearing (existing)
Axial Length (*in*)	1.0	1.0	1.0	1.0
Journal Diameter (*in*)	1.3185	1.3185	1.3185	1.3185
Bearing Clearance (*in*)	0.0015	0.0015	0.0015	0.0015 (inner) 0.0025 (outer)
Preload (*dim*)	0	0.5	0.5	0
Offset (*dim)*	0	0.5	0.5, 0.65	0

The compressor-side bearing is of primary interest due to all damage in failed turbochargers having place on the compressor side. Table 2.4 contains the information used to establish the data files for the turbine side bearings.

Table 2.3b: Dimensions of Comparative Bearings, Turbine Side

Dimension	Plain Journal Bearing	4-Axial Groove Bearing	4-Tilting Pad Bearing	Floating Axial Groove Bearing (existing)
Axial Length (*in*)	1.0	1.0	1.0	1.0
Journal Diameter (*in*)	1.693	1.693	1.693	1.693
Bearing Clearance (*in*)	0.0015	0.0015	0.0015	0.0015 (inner) 0.0025 (outer)
Preload (*dim*)	0	0.5	0.5	0
Offset (*dim)*	0	0.5	0.5, 0.65	0

Finally, to maintain a realistic model, an unbalance was added to the rotor utilizing American Petroleum Institute (API) standards for maximum unbalance which is governed by the equation:

$$U_{oz-in} = \frac{4W}{N} \tag{2.1}$$

Where: U acceptable unbalance, ounce-inches
W mass of rotor
N Rotational speed of rotor, RPM

It is determined that a maximum unbalance of 0.006 oz-in is permissible in this rotor.

Static bearing conditions were considered in the DyRoBeS BePerf program for calculation of stiffness and damping values. The static loads were determined by DyRoBeS Rotor considering the rotor generated for analysis and are contained in Table 2.4.

Table 2.4: Static Bearing Loading Conditions

Bearing	Bearing Station	Static Load (lb_f)
Turbine	3	18.3
Compressor	7	25.8

2.3 *Modeling of the Hybrid Floating Axial Groove bearing*

The "Floating 4-Axial Groove Bearing" is not an option for modeling in the DyRoBeS system, likely due to this bearing design's lack of popularity. In generating a model to provide bearing characteristics to the DyRoBeS Rotor program, a critical assumption must be made in the DyRoBeS BePerf program. It is known that a floating ring bearing can be accurately modeled as two plain journal bearings placed in series, separated by a mass equal to that of the floating ring itself [9]. This method of solving more complex bearing problems has been used in

previous editions of DyRoBeS BePerf prior to later releases which implemented this capability internally. It is reasonable, then, to assume that a floating axial groove bearing may be approximated as an axial groove bearing in series with a plain journal bearing, separated by a mass equal to that of the floating axial groove ring. The key to this approximation is to properly incorporate the speed ratio of the floating ring. As discussed in previous sections, the relative speed is the critical component when determining bearing characteristics. Running various simulations of the bearing configuration have yielded a repeatable approximation of the speed ratio as thirty percent. That is, the floating ring spins with an angular velocity of approximately 30% of that of the journal. While a speed ratio of 50% is ideal, this is rarely achieved, largely due to the higher temperature, and thus lower viscosity, of the inner film. As discussed, the characteristics of the fluid film are dependent upon the relative velocity between two surfaces; with the floating ring spinning at 30% of the journal velocity, the *effective* velocity of the inner bearing surface is only 70% that of the actual journal speed.

Because there is no option to generate the actual bearings of this model in DyRoBeS directly, a bearing data file was generated as a ".brg" document (DyRoBeS file type for bearing characteristics) defining a four axial groove bearing with the dimensions found in the model. It was determined that a .brg file can be accessed and modified as a ".txt" file in the computer's notepad, so long as the proper formatting is maintained as demanded by DyRoBeS. The specific modification needed to maintain the proper axial groove bearing characteristics is to divide each speed in the data file by 0.7 (as discussed, the relative speed between the converging surfaces is critical, if the ring is rotating at 30% of the speed of the shaft, the relative speed is 70%). For example, a journal must rotate at 1000 rpm to have the inner-film characteristics of a journal rotating at 700 rpm. Characteristics in the new .brg file are indexed by the actual journal speed

(the higher of the two) however contain data for the lower, relative speed. An excerpt of this modification is visible in Table 2.5.

Table 2.5a: Compressor Bearing Characteristics as Calculated, Relative Speed

	Kxx	Kxy	Kyx	Kyy
700	3.2376E+004	2.26426E+004	-5.19721E+004	5.92332E+004
1400	3.62903E+004	3.37363E+004	-5.67518E+004	5.18655E+004
2100	3.75498E+004	3.87338E+004	-5.76354E+004	5.04784E+004
2800	3.93787E+004	4.47586E+004	-5.92014E+004	4.87862E+004

Table 2.5b: Compressor Bearing Characteristics as Entered, Actual Speed

	Kxx	Kxy	Kyx	Kyy
1000	3.2376E+004	2.26426E+004	-5.19721E+004	5.92332E+004
2000	3.62903E+004	3.37363E+004	-5.67518E+004	5.18655E+004
3000	3.75498E+004	3.87338E+004	-5.76354E+004	5.04784E+004
4000	3.93787E+004	4.47586E+004	-5.92014E+004	4.87862E+004

DyRoBeS BePerf's capability to analyze floating ring bearings did become useful to finish the approximation. The outer fluid film between the floating ring and the outer bearing housing was easily approximated by treating the bearing as a typical floating ring bearing. DyRoBeS generates three sets of data for each of these bearings: the inner coefficients, the outer coefficients, and the equivalent coefficients. Each of these data files can be accessed individually. When the bearing data is entered into the DyRoBeS Rotor program, four bearings and 2 masses must be defined. The inner fluid film (closest to the rotor) is defined by the modified data set, the mass is calculated using the ring dimensions and the density of the material (bronze), and the outer film is defined directly from the outer film data file provided by DyRoBeS-BePerf. This procedure is repeated for the second bearing station on the rotor. This

concept is visible in Figure 3.1; note the locations of the turbine and compressor bearings at stations 3 and 7, respectively.

CHAPTER 3

STABILITY ANALYSIS

3.1 *Scope of Analysis*

The first analysis to take place was the study of the static loading of the bearings, which is available in the DyRoBeS Lateral Analysis option. While this analysis isn't itself directly indicative of system stability, it gives an overall feel for where the forces of the system are located. It was determined that the turbine bearing, being the larger of the two bearings, is loaded only to 18 pounds, while the small compressor bearing is loaded to 26 pounds. While it is interesting that the smaller bearing is more heavily loaded, both bearings are capable of supporting the static loading condition. A quick check confirming this capability conservatively uses the short bearing equation. The requirement for the short bearing method is that $\frac{L}{R_1} \ll 1$, where L is the axial length of the bearing, and R_1 is the radius of the bearing. This requirement is not met, although will provide a calculated load capacity lower than that of the actual bearing, since axial flow is being neglected. The simplified load capacity approximation is [16]:

$$W = \mu \Omega R L \left(\frac{L}{C}\right)^2 \frac{\varepsilon}{4} \frac{\sqrt{16\varepsilon^2 + \pi^2(1+\varepsilon^2)}}{(1-\varepsilon^2)^2} \tag{3.1a}$$

where μ lubricant viscosity
Ω rotational speed (rpm)
L bearing length
C bearing clearance on radius
ε eccentricity ratio (approximated using DyRoBeS BePerf)
R bearing radius

yielding:

$$\Omega = \frac{W}{\mu R L \left(\frac{L}{C}\right)^2 \frac{\varepsilon}{4} \frac{\sqrt{16\varepsilon^2 + \pi^2(1+\varepsilon^2)}}{(1-\varepsilon^2)^2}} \approx 735\, rpm \tag{3.1b}$$

So, at only 800 rpm, the static load of 26 pounds is supported. The shaft speed would be expected to be greater than 800 rpm even at idle conditions, and thus the static loading of the bearing is not excessive. Any excessive deflection will be caused by forces resulting from instabilities.

It is believed that this bearing configuration exists to allow for removal of the turbocharger cartridge without removing the entire housing. The turbocharger "cartridge" consists of the bearings and rotating assembly (shaft, turbine, thrust collar, and compressor). The turbine is welded to the shaft, while the compressor is held in place with a bolt; this bearing configuration allows the cartridge to be removed through the turbine side of the housing after unbolting the compressor wheel [17].

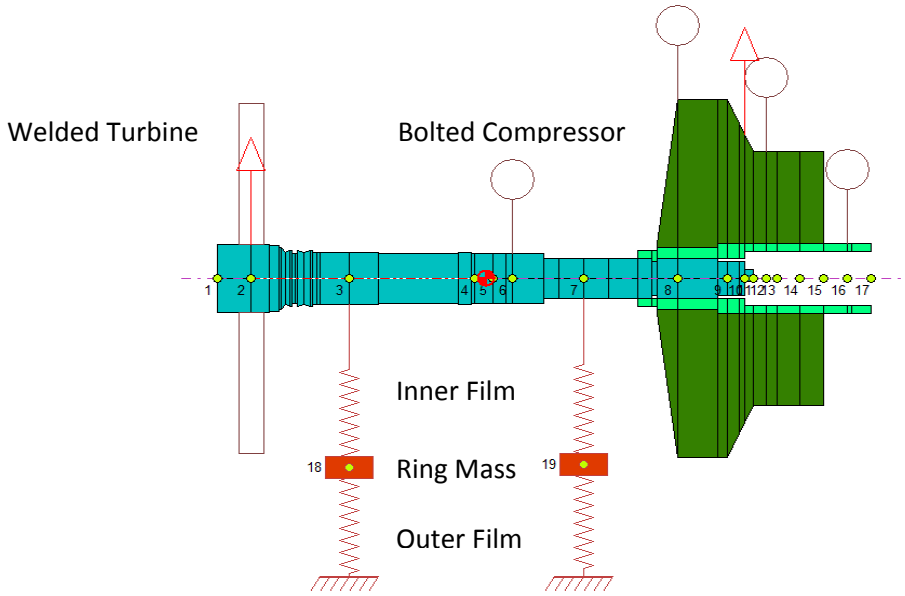

Figure 3.1: Floating Ring Bearing Formation

A stability analysis often focuses on the logarithmic decrement (log dec) of the system, that is, the system's overall effective damping ratio. A well-damped system will have a logarithmic decrement greater than 1, while an unstable system will have a negative logarithmic

decrement. The logarithmic decrement is calculated by DyRoBeS and by definition is the natural log of the ratio of successive peak amplitudes of vibration in a transient state. The equation is easier to follow.

$$Log\ Dec = \delta = ln\left(\frac{x_i}{x_{i+1}}\right) \tag{3.1a}$$

where δ logarithmic decrement
x_i amplitude of vibration at cycle i
x_{i+1} amplitude of vibration at cycle i+1

It can be shown that logarithmic decrement can also be reduced from the vibrations equation of motion to take the form:

$$\delta = \frac{2\pi\zeta}{\sqrt{1-\zeta^2}} \tag{3.1b}$$

Where:

$$\zeta = \frac{C}{C_c} \quad C_c = 2Mw_n = 2\sqrt{KM}$$

and where M mass
C damping
K stiffness
δ logarithmic decrement
ζ damping ratio

It is also useful to study the vibration amplitudes at various stations of the rotor. Four particular stations have great significance- the 2 bearing stations and the station at the turbine disk and at the compressor disk. The vibration amplitudes compared to the clearances at these stations will quickly identify failure potential. Contact of either wheel with the outer turbocharger housing would send the rotor into an unstable whirl, while also contaminating the lubricating oil of the bearings with debris, almost certainly resulting in immediate turbocharger failure. Contact at the bearing stations could result in various series of events, ultimately resulting in failure as well.

The ABB VTC 254 has a large clearance around the wheels- nearly a quarter of an inch- so it is unlikely that contact would take place at these locations prior to a major failure elsewhere. The bearings, on the other hand, have a total clearance (inner plus outer) of only 0.0065", or 6.5 mils, assuming a standard 5 mil clearance in the outer bearing. It will be shown, using the conservative approach of linear approximations, that the turbocharger cannot survive routine operation. As results of various bearing configurations are discussed, it is important to remember that the rotor model itself is identical for every simulation, and that only the bearing characteristics are varied.

3.2 *Analysis of Existing Configuration*

As discussed, the existing configuration of the turbocharger consists of the main rotor supported by a pair of four-axial groove floating ring bearings as seen in Figure 2.1. The stability of the rotor is studied at various speeds, and is defined by the logarithmic decrement. The turbocharger operates at a speed range between 10,000 and 30,000 rpm, so the speeds identified for analysis are 15,000, 23,000, and 30,000 rpm. These values will provide data for realistic operating speeds resulting from various engine loading conditions. Resulting logarithmic decrement values and mode shapes for the floating axial-groove bearing are shown in Figure 3.2 a-c.

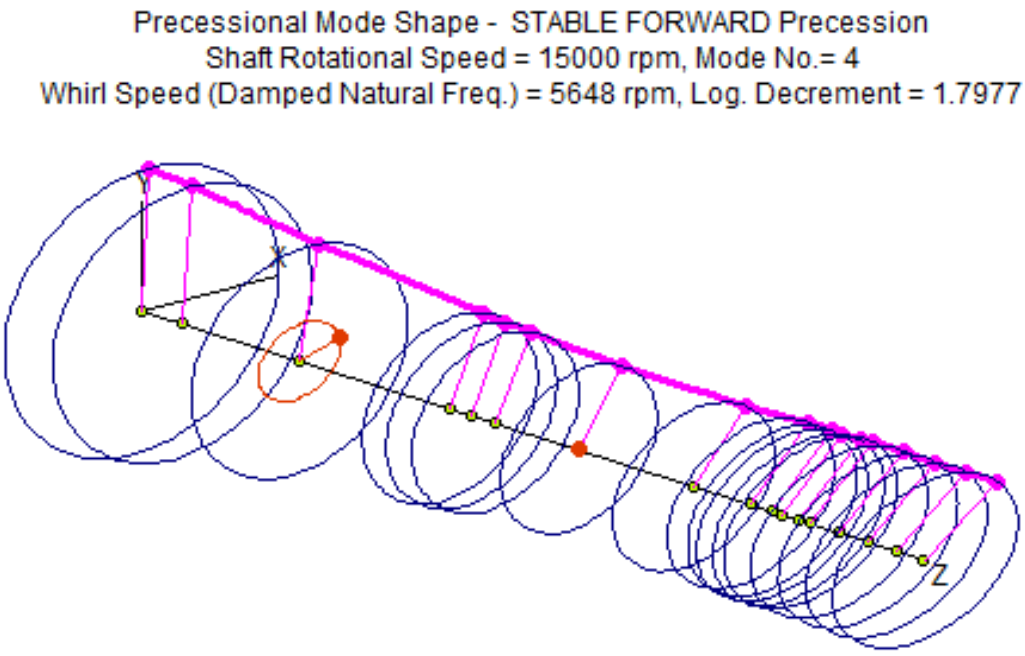

Figure 3.2a: Stable forward precession with floating axial groove bearings at 15,000 rpm.

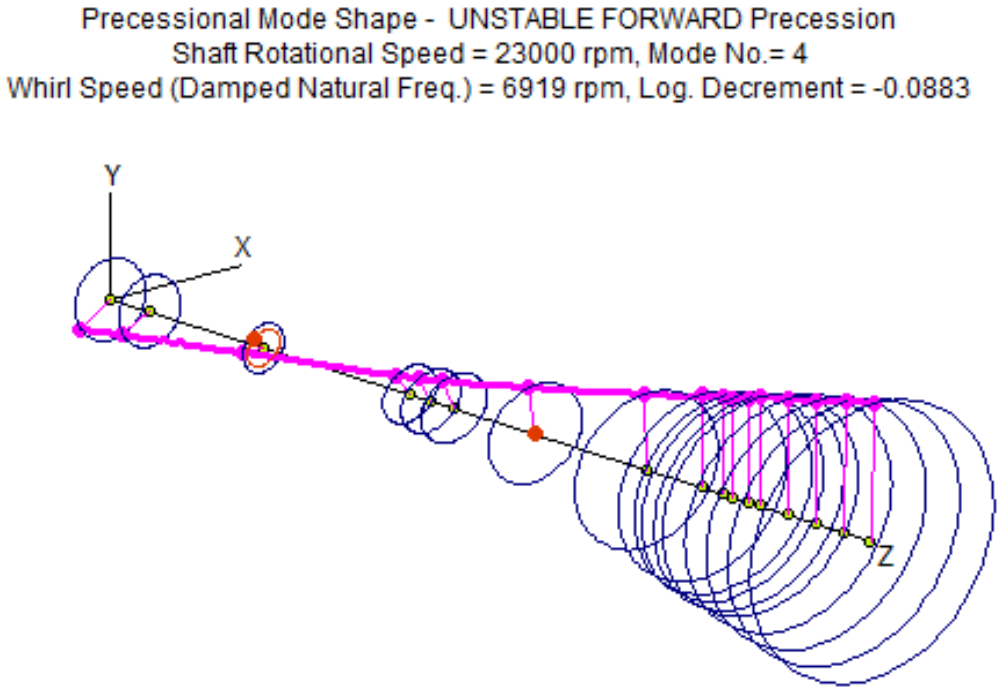

Figure 3.2b: Unstable forward precession with floating axial groove bearings at 23,000 rpm.

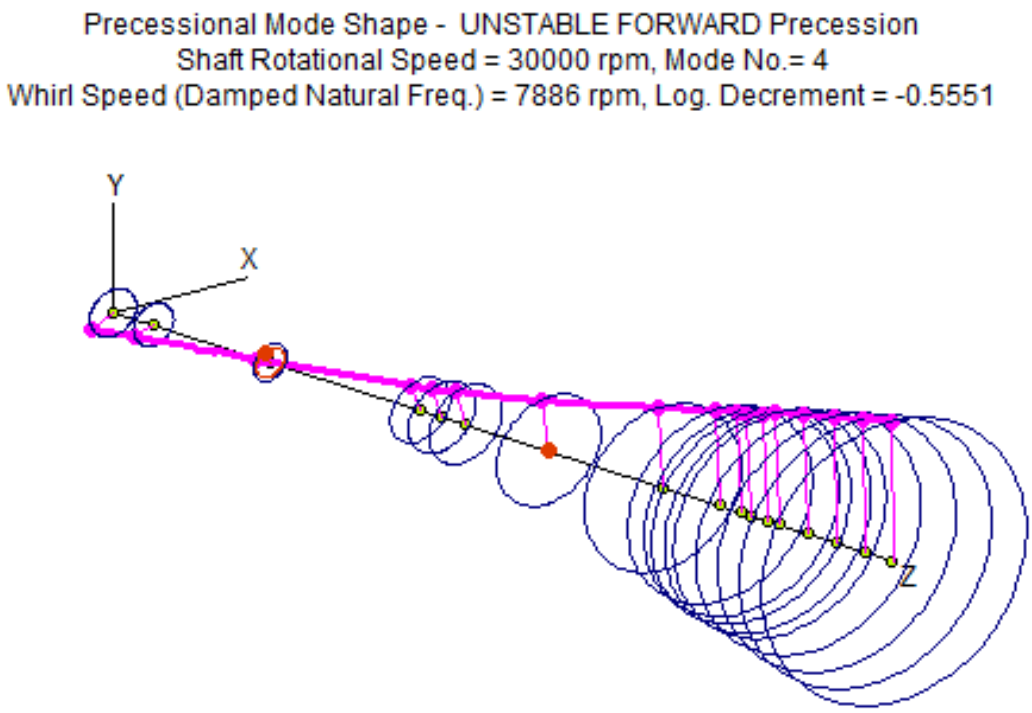

Figure 3.2c: Unstable forward precession with floating axial groove bearings at 30,000 rpm.

As can be seen in Figures 3.1, the turbocharger operates in a stable condition through 20k rpm, but exhibits unstable characteristics at the 23k rpm model. At full designed operating speed, the rotor exhibits stronger unstable sub-synchronous whirling. Additionally, many of the higher bending modes have a logarithmic decrement of only 0.01 or less, one of which is visible in Figure 3.3. These modes could turn unstable with simple variances in assembly or machining tolerances, or even with reduced viscosity associated with increased operating temperatures.

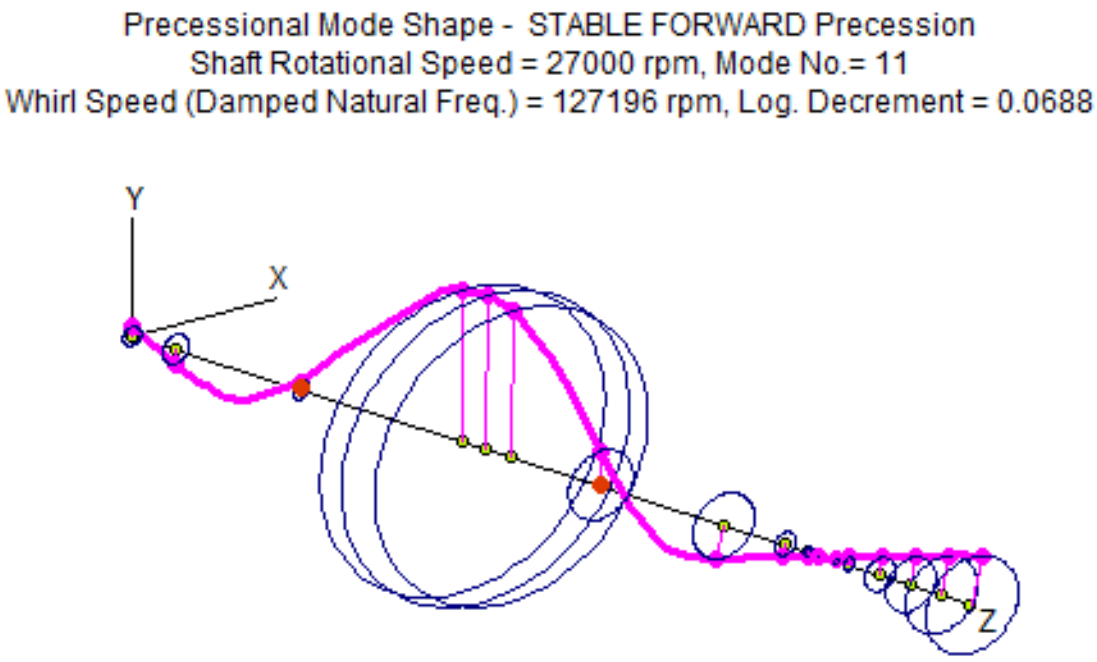

Figure 3.3: Marginally stable third bending mode with floating axial groove bearings.

In addition to the mode shapes and logarithmic decrements calculated in Figures 3.2 a-c and 3.3, a stability map is useful when the modal information is not critical. A stability map is visible below in Figure 3.4, values below the red line (where logarithmic decrement equals zero) indicate instabilities. Each individual series of data represents the logarithmic decrement of an individual mode at various speeds.

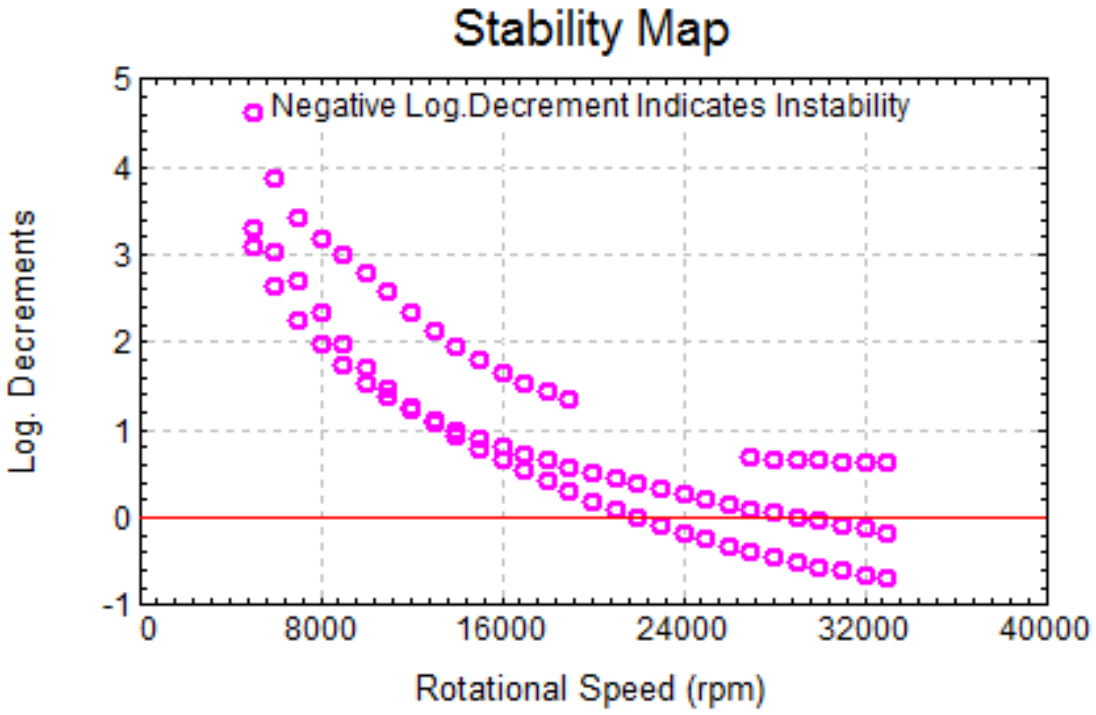

Figure 3.4: Stability Map of rotor with floating axial groove bearings.

3.3 *Analysis of Existing Rotor, Seized Floating Ring*

In addition to the unstable whirling of the rotor in its existing configuration, the analytical shaft deflection appears to be within permissible limits at the location of the wheels, but indicates a high risk of rub at bearing locations. The calculated displacement of the journal center is visible in the Displacement Orbit map of Figure 3.5. When viewing the Displacement Orbit map, the whirl displacement will be compared to the bearing clearance. While tighter clearances were assumed to generate higher bearing stiffness and damping values to decrease the chance of falsely identifying an unstable condition, the greatest total clearance of this configuration is 0.0065 inches. This information will be of further use when discussing the potential of a "seized-ring" condition, where the floating ring becomes seized to the journal.

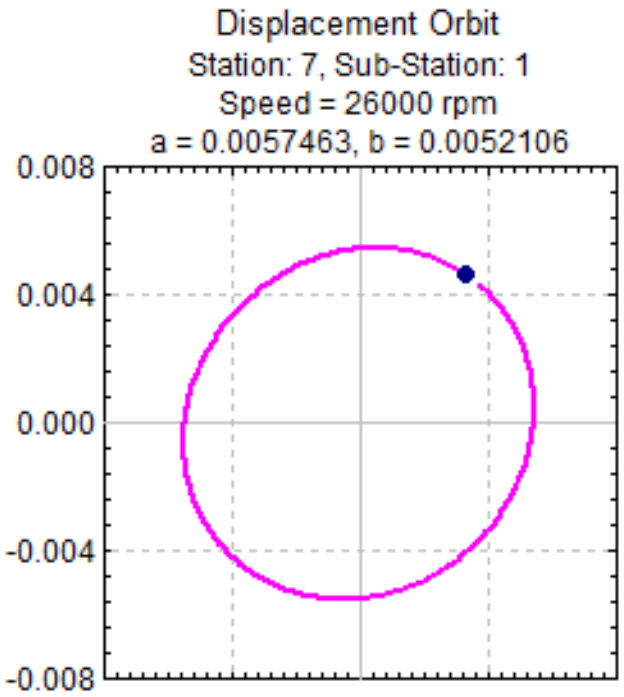

Figure 3.5: Displacement orbit of rotor with floating axial groove bearings at 26k rpm.

As the vibration amplitude of the journal increases, the oil temperature of the inner film will increase, reducing viscosity and thus stiffness. The high stiffness value of the outer fluid film will suppress the motion of the floating ring. The combination of these two events presents a realistic possibility that the floating ring may become seized to the journal. It can be shown that contact between the journal and floating ring are likely in this method of operation. Figure 3.5 indicates that the journal is expected to vibrate with amplitude of approximately 6 mils, while the total bearing clearance is only 6.5 mils. The remaining clearance of only 0.5 mils is quickly consumed by the increase in temperature of the journal. The permissible temperature difference between the journal and outer housing, then, can be calculated by equation 3.2, below.

$$L = \alpha L_1 \Delta T, or\ \Delta T = \frac{L}{\alpha L_1} \tag{3.2}$$

Where: L Initial Length (circumference, in)

L_1 Permissible change in length (circumference, in)

α Thermal expansion coefficient $\left(\frac{in}{in-°F}\right)$ [18]

$$\Delta T = \frac{0.0015\pi}{6.5 * 10^{-6}(5.809)} = 125°F$$

The thermal expansion of the floating ring is not considered due to the increase of its inner diameter being very similar to that of the outer diameter, only the reduction in clearance between the journal and outer housing is considered in this situation. The inner film, with the much tighter clearance, will have a much lower viscosity than that of the outer film due to the increased operating temperatures. This lower viscosity makes the risk of contact of the journal with the floating ring higher than that of the floating ring with the outer housing. A temperature difference of only 125 degrees Fahrenheit is not unreasonable, thus seizure of the floating ring to the journal is considered to be likely. The temperature of the oil through an axial groove bearing is shown in Figure 3.6.

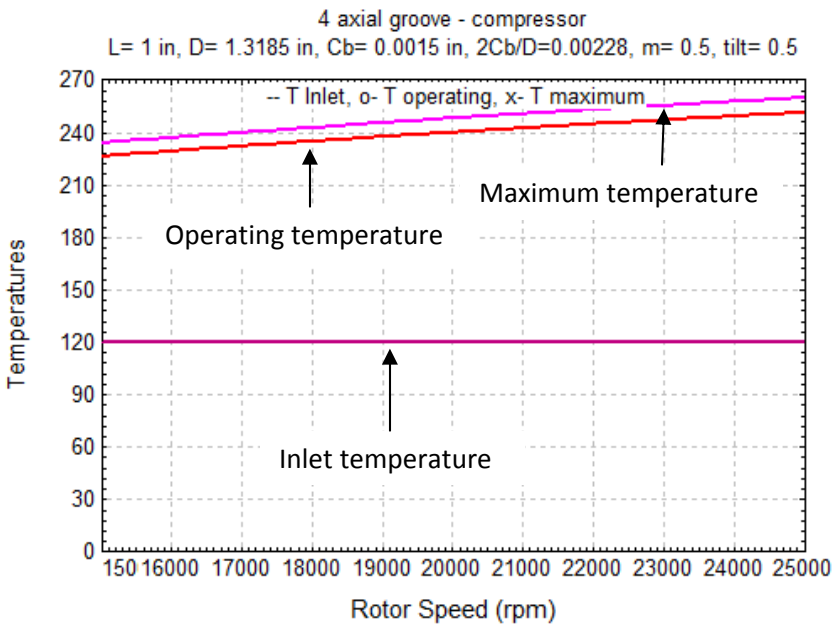

Figure 3.6: Temperature rise of oil through 4 axial groove bearing.

In this event, the floating axial groove bearing takes on the characteristics of a large clearance plain journal bearing. It has been discussed that most journal bearings permit approximately 0.0015 inches of clearance per inch of journal diameter. In this case, the higher flow of oil over the outer surface of the floating ring would significantly reduce thermal expansion of the ring, and the clearance between the journal and outer bearing housing would be approximately 0.005 inches, or about three times the standard clearance. Excessive clearances in the fluid film will encourage greater oil whirl and thus stronger cross-coupled instability forces. Examination of the mode shapes and logarithmic decrements of the rotor with this large-clearance plain journal bearing reveals strong instabilities, represented in Figures 3.7 a-c and 3.8.

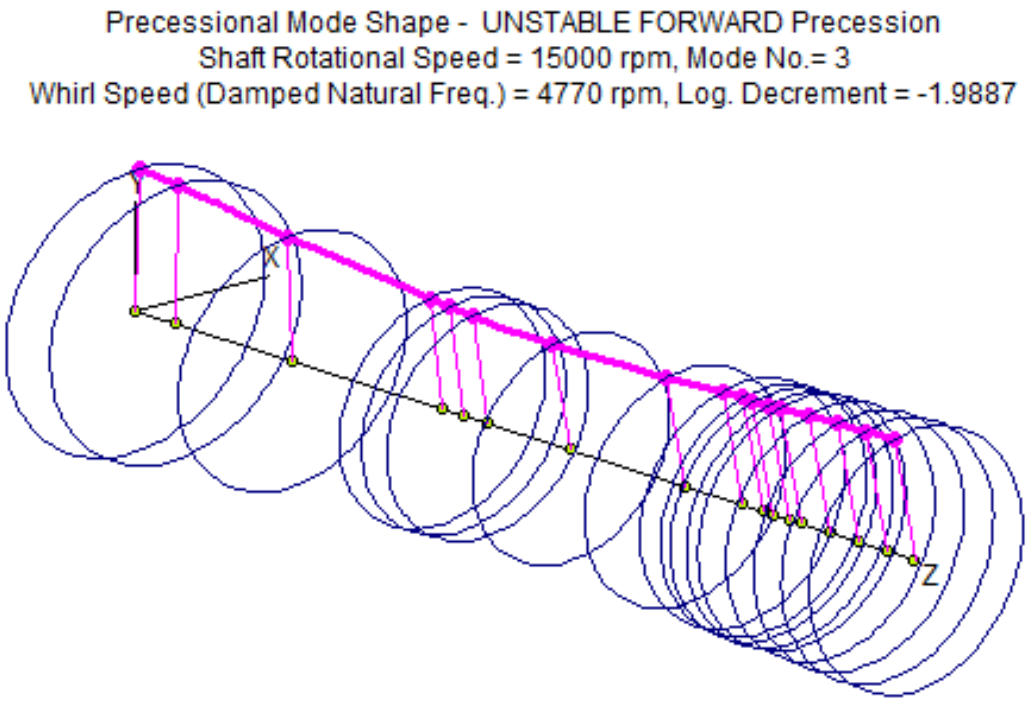

Figure 3.7a: Unstable precession of large clearance plain journal bearing at 15k rpm.

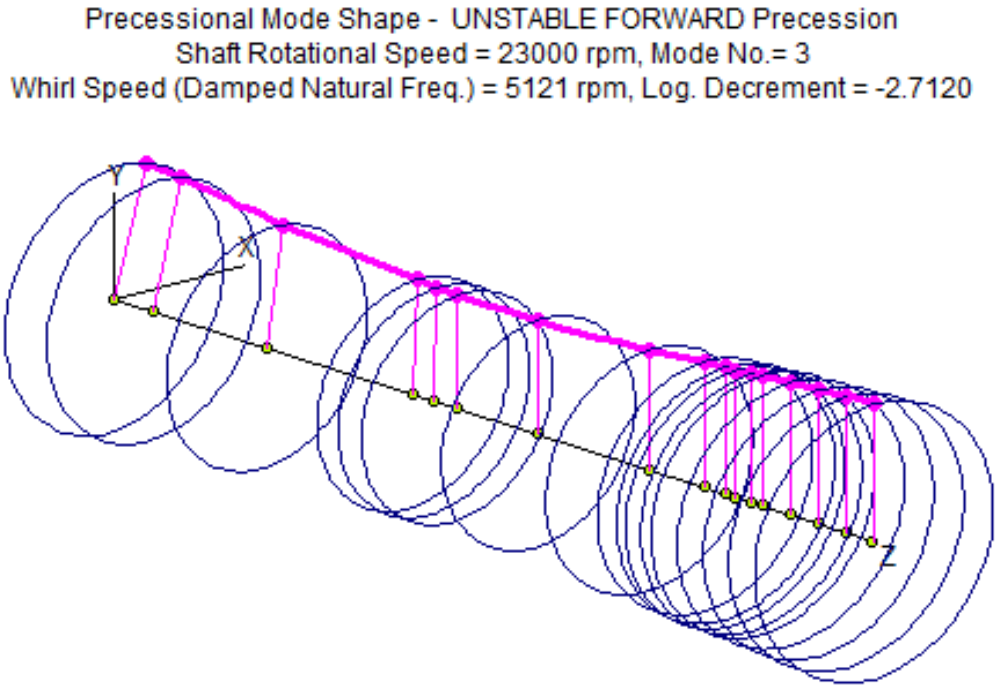

Figure 3.7b: Unstable precession of large clearance plain journal bearing at 23k rpm.

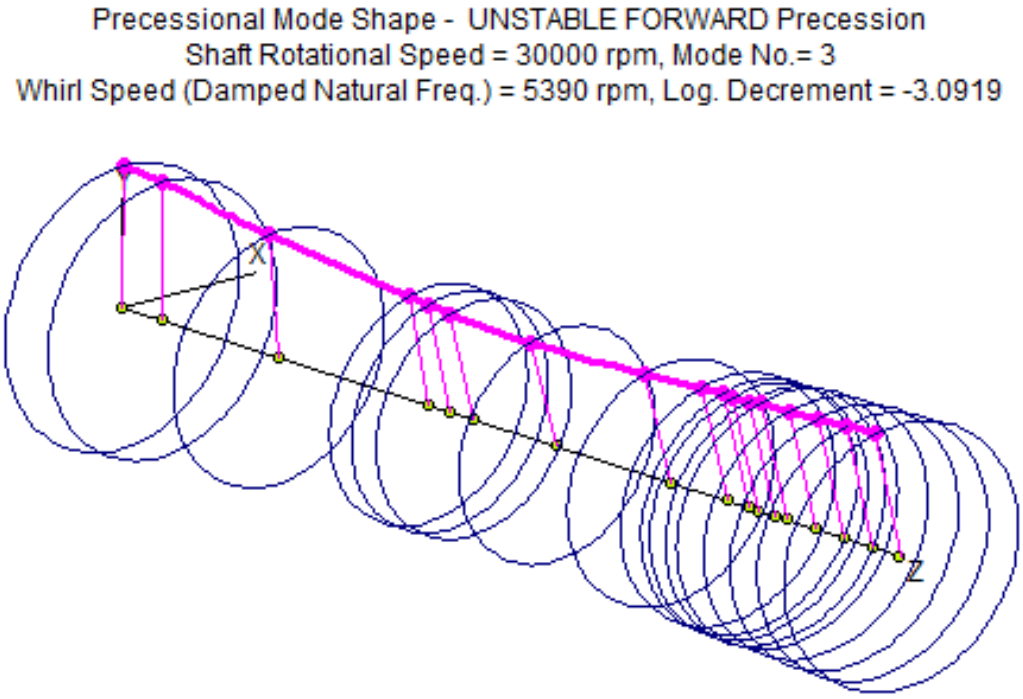

Figure 3.7c: Unstable precession of large clearance plain journal bearing at 30k rpm.

Figures 3.7 a-c indicate that the rotor will undergo strong sub-synchronous whirling. As was the case with previous bearing considerations, this instability is again visible over a majority of the operating speed range in the stability map in Figure 3.8. It will be shown that although the floating axial groove bearing design exhibits better stability than most fixed-geometry bearing designs, the high risk of the floating ring seizing to the shaft results in an extremely unstable system.

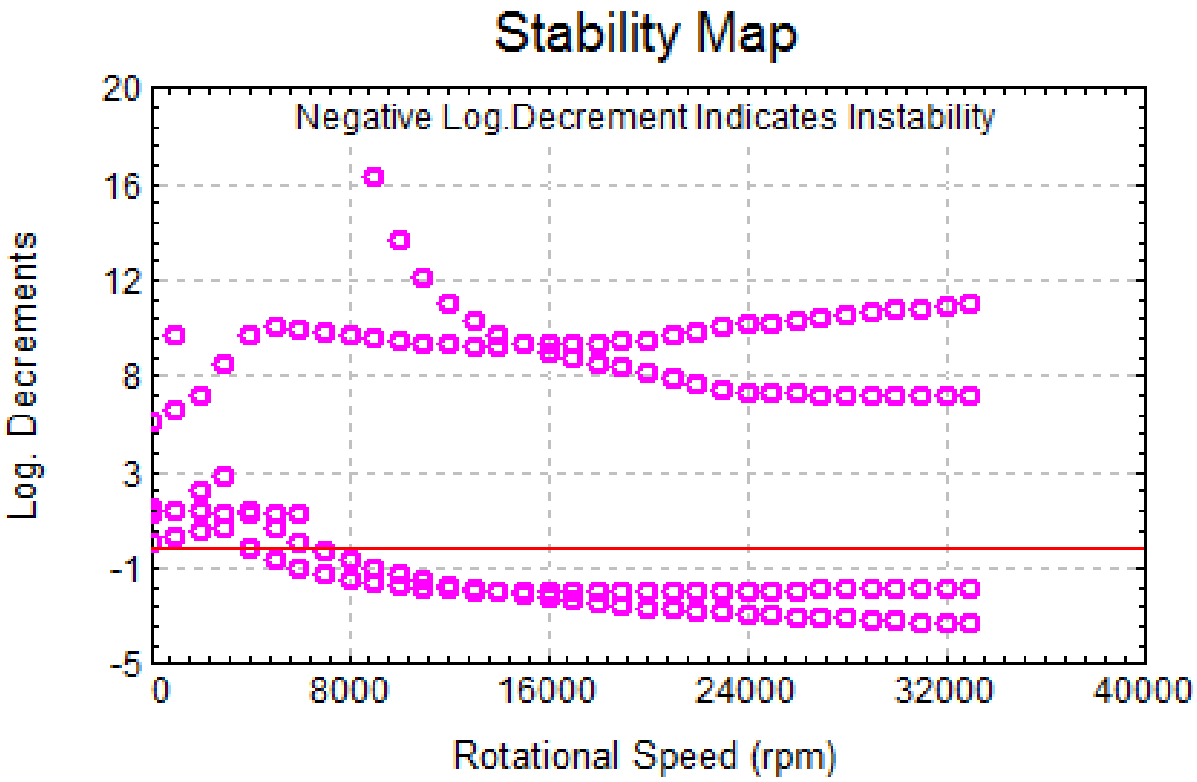

Figure 3.8: Stability Map of rotor with large clearance plain journal bearings.

It is apparent in the stability map that unstable precession exists not only at the speeds previously defined, but throughout the entire operating range of the turbocharger once the floating bearing seizes to the journal.

3.4 *Analysis of Rotor with Standard Floating Ring Bearings*

With a thorough explanation of the existing turbocharger configuration as well as that of the seized bearing having already been discussed, it becomes appropriate to discuss similar, yet different options which could have been implemented. The standard floating ring bearing will be presented as well as the standard four axial groove bearing; these two bearings combined form the actual bearing found in the turbocharger. It will be shown that these bearings each have

similar flaws to the floating axial groove bearing; chapter four will introduce an appropriate bearing design capable of properly supporting this rotor.

The standard floating ring design has similar dimensions to the floating axial groove design, with the exception of the absence of the axial grooves on the inner diameter of the ring. After examining the mode shapes and logarithmic decrements at the defined speeds, visible in Figure 3.9, it is apparent that the floating axial groove bearing is stable only slightly further into the operating range than the standard floating ring bearing; however, both ultimately exhibit unstable characteristics within the rotor's operating range.

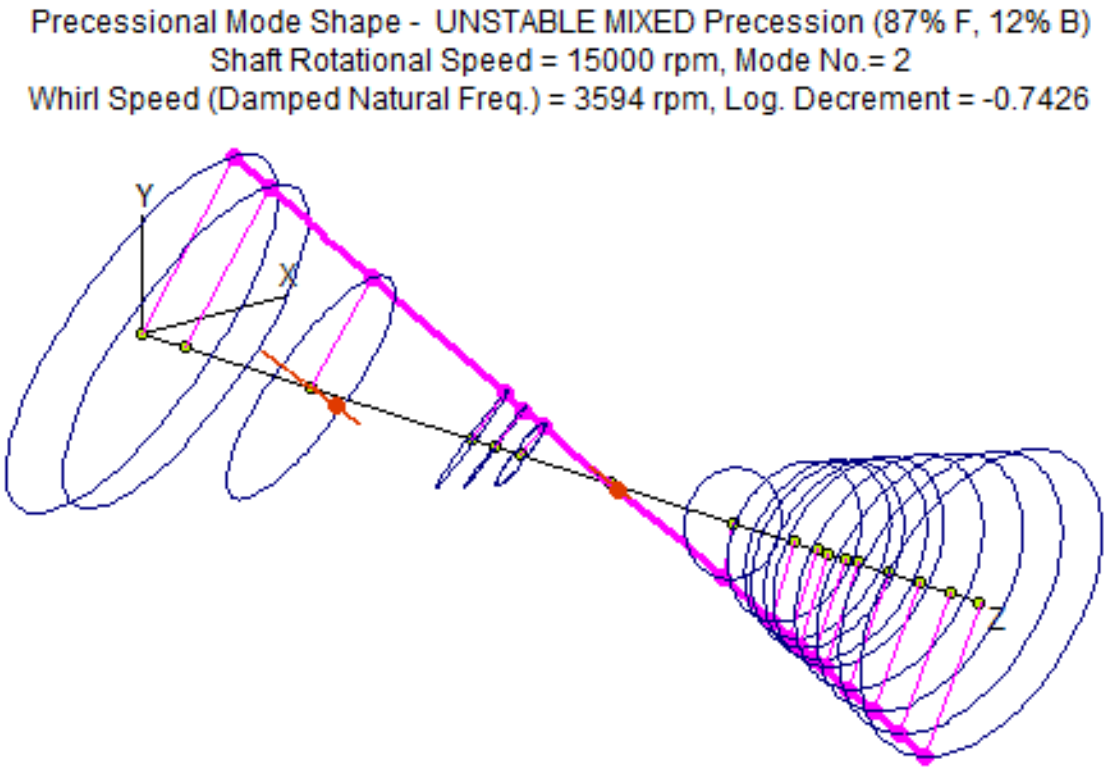

Figure 3.9a: Unstable precession of rotor with standard floating ring bearings at 15k rpm.

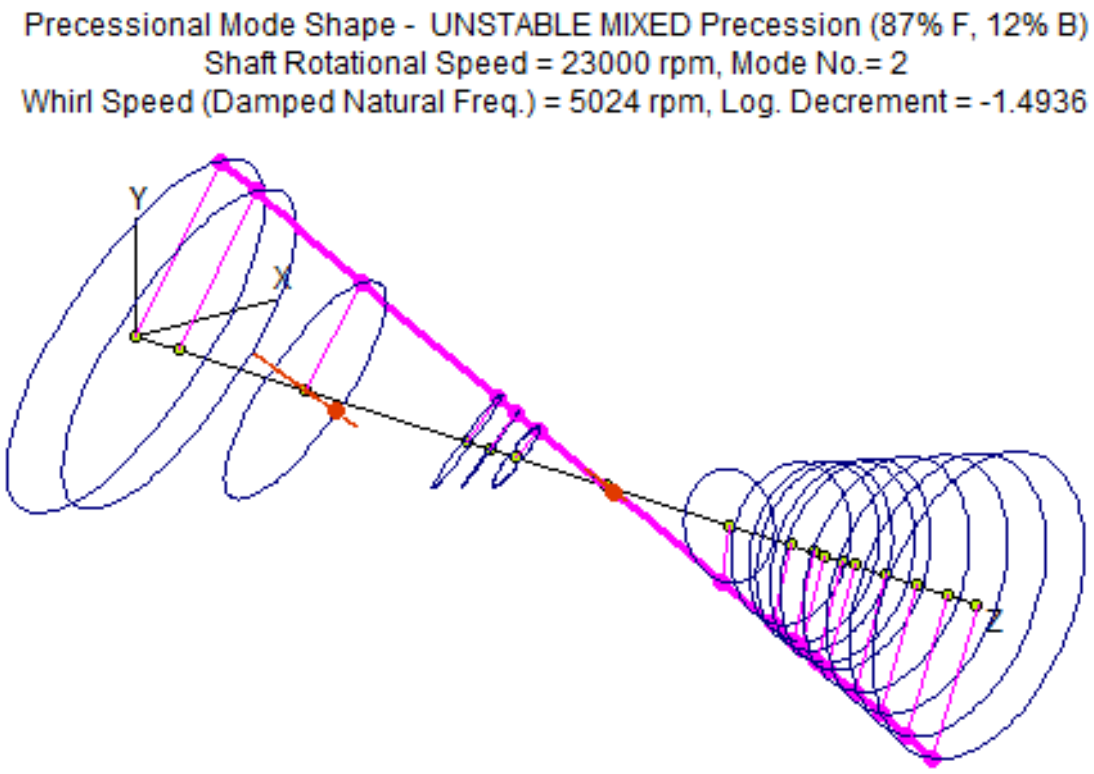

Figure 3.9b: Unstable precession of rotor with standard floating ring bearings at 23k rpm.

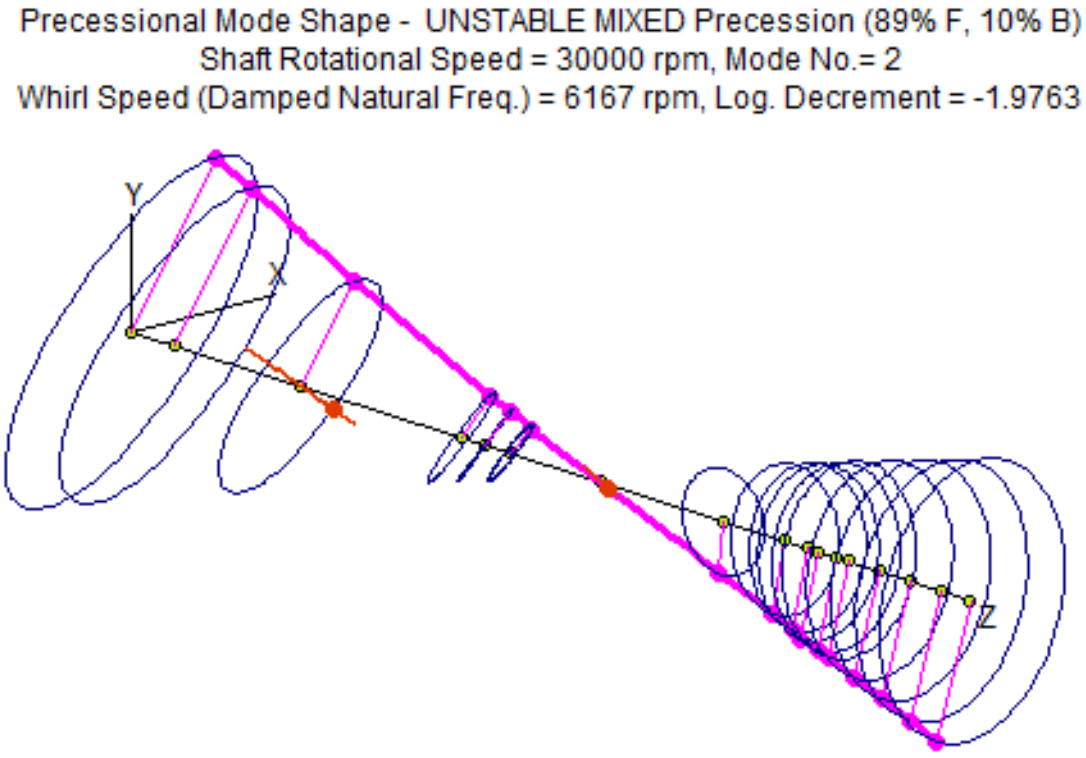

Figure 3.9c: Unstable precession of rotor with standard floating ring bearings at 30k rpm.

In addition to the instabilities at the referenced speeds, again the stability map in Figure 3.10 indicates unstable characteristics throughout the entire operating range. It becomes apparent that the self-induced excitation of the shaft cannot be supported by any form of the floating ring bearing.

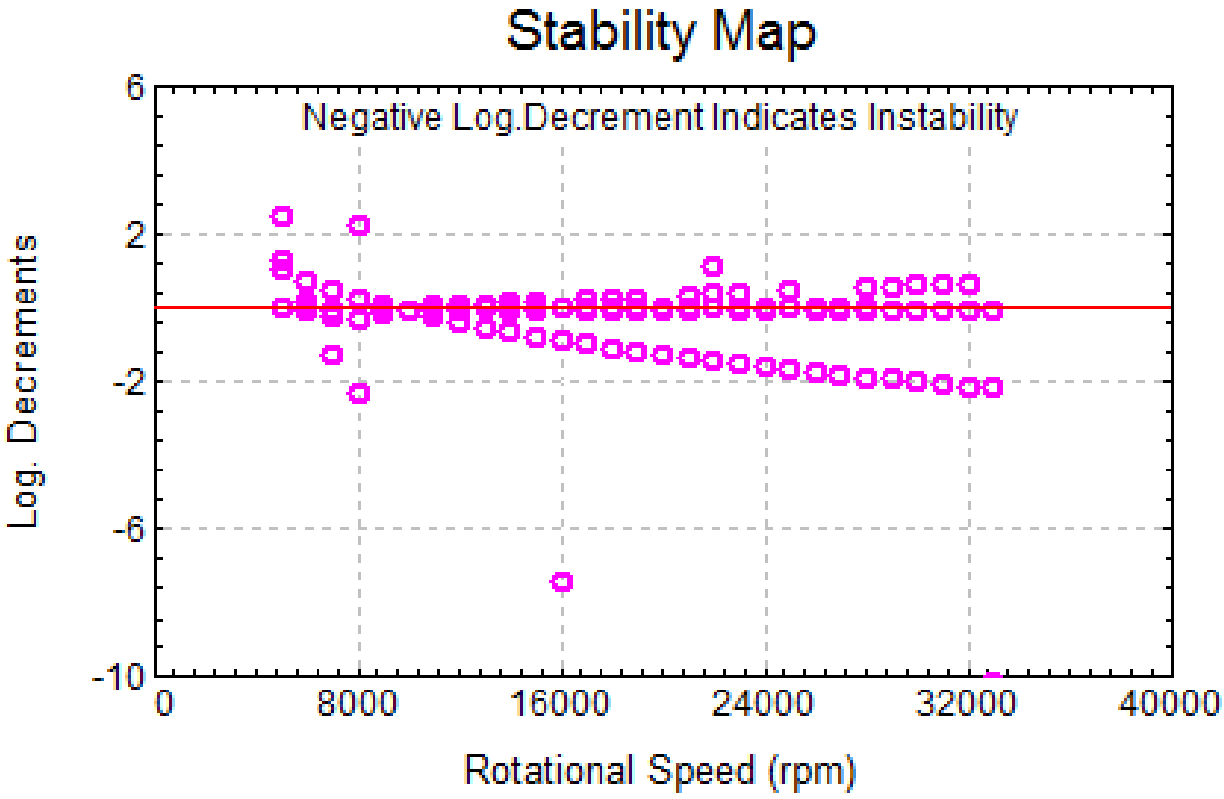

Figure 3.10: Stability map of rotor with standard floating ring bearings.

3.5 *Analysis of Rotor with Standard Axial Groove Bearings*

Lastly, since the floating ring itself is actually an axial groove bearing, it was decided to model the rotor as if it contained standard floating ring bearings. As was discussed, the dynamics of this rotor will reflect a combination of characteristics of both the floating ring bearing and the axial groove bearing. As has been the trend with other bearing configurations

thus far, the rotor exhibits unstable characteristics throughout its operating range, primarily in the rigid body modes, shown in Figure 3.11 a-c.

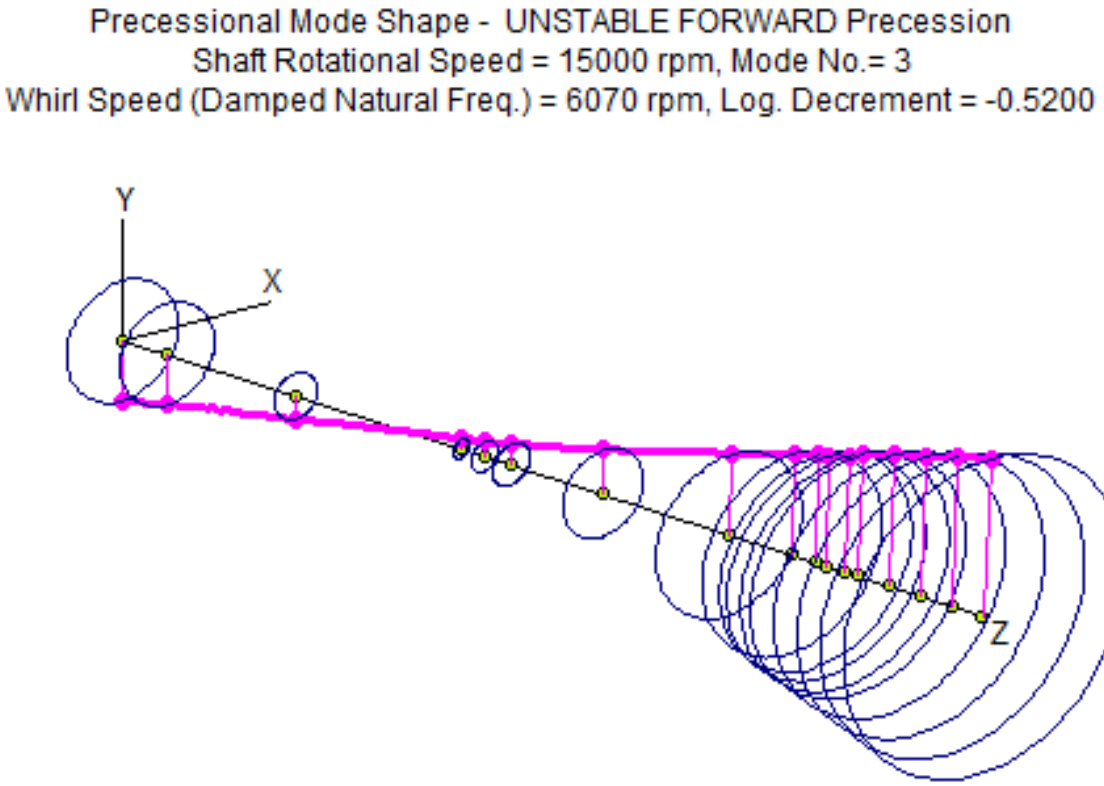

Figure 3.11a: Unstable precession of rotor with standard axial groove bearings at 15k rpm.

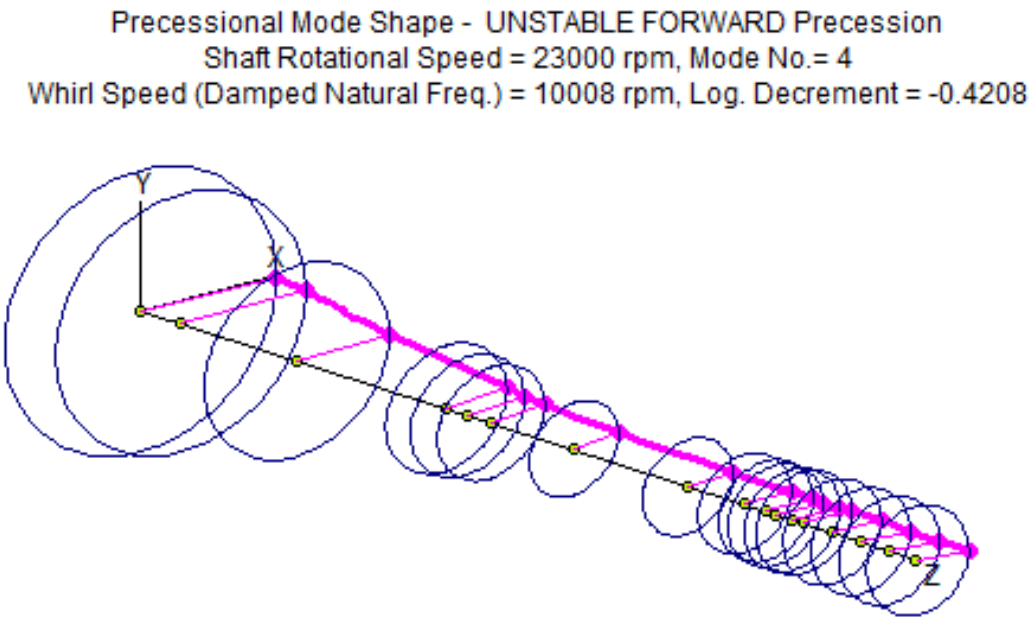

Figure 3.11b: Unstable precession of rotor with standard axial groove bearings at 23k rpm.

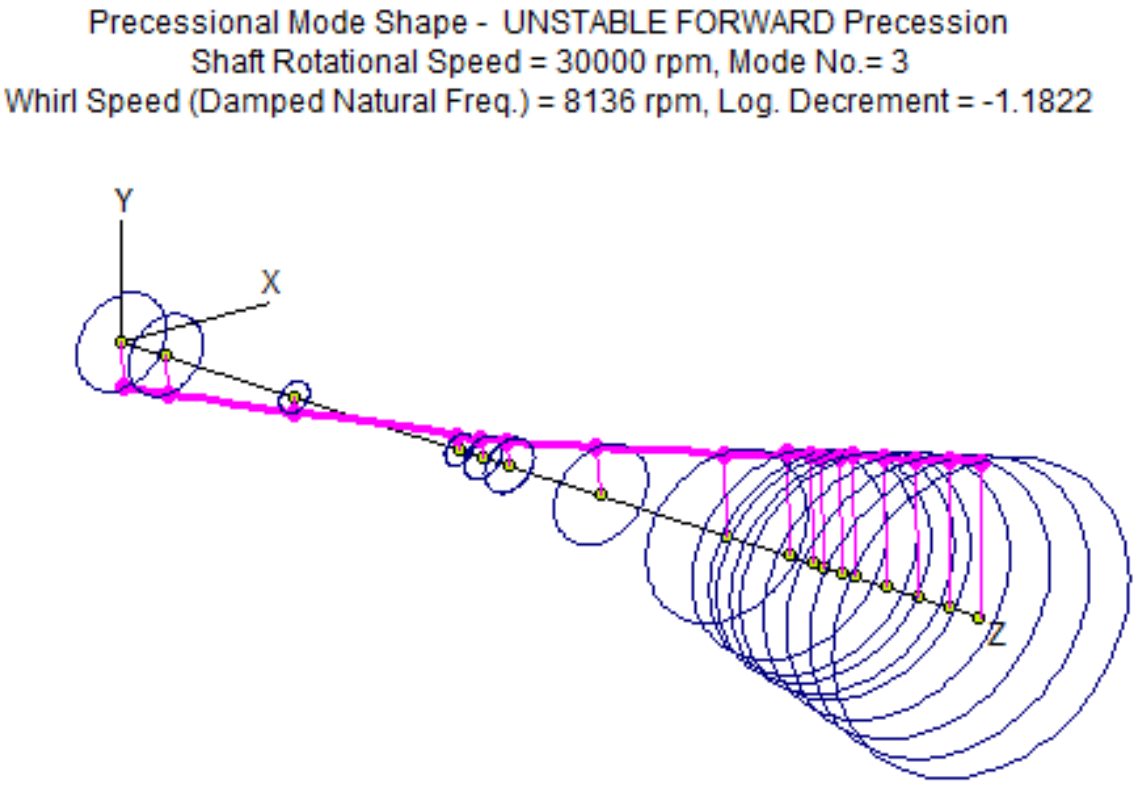

Figure 3.11c: Unstable precession of rotor with standard axial groove bearings at 30k rpm.

Again, in addition to the unstable precession at the defined rotor speeds, the stability map was generated to get a better feel for the overall stability trend of the rotor. The stability map, as expected, demonstrates unstable characteristics throughout the operating range of the rotor, shown in Figure 3.12.

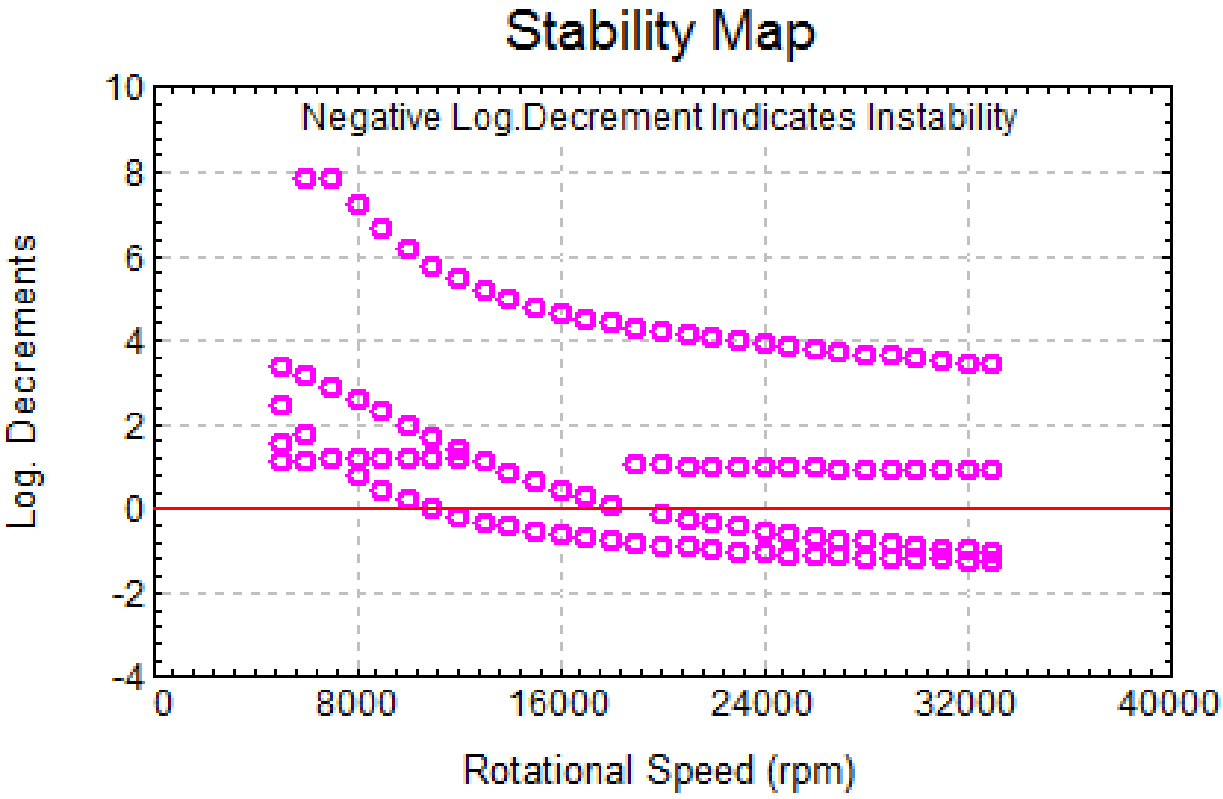

Figure 3.12: Stability map of rotor with axial groove bearings.

Having modeled the rotor with a series of typical bearing designs, it becomes apparent that this rotor is in need of a more resilient bearing. While a pressure dam bearing could be considered, the weight of the rotor itself is significant, so adding an artificial weight (downward force) is impractical. Reversing the pressure dam bearing by placing the dam on the bottom and the relief on the top would defeat the purpose of the bearing design. In following typical industry standards, the best bearing design for this application would be the tilting pad bearing.

CHAPTER 4

STABLE BEARING RECOMMENDATIONS

4.1 *The Tilting Pad Bearing*

The Tilting Pad bearing was introduced in Chapter One as one of the most advanced bearing designs currently on the market. In its most simple form, the tilting pad bearing is similar in operation to the multi-lobe bearing with one difference: the pads are free to tilt and conform to the displacement of the journal. The stability of a rotor-bearing system may be greatly increased by altering preload and offset values, as well as considering pad effects. The alteration of offset must be made with knowledge of the system, for any reverse rotation will result in a diverging clearance between the journal and bearing creating instabilities. Reverse-rotation on a turbocharger would require a greater pressure on the discharge side of the turbine, which is typically open to the atmosphere creating very little back-pressure, than the inlet side. The inlet side of the turbine will have a maximum possible pressure equal to the discharge pressure from the engine's cylinders. A reasonably designed turbocharger system has no chance of reverse rotation; an offset can be safely applied if desired.

Figure 4.1 shows a schematic of a tilting pad bearing. Not that the pivot point of the pads is not at the center of the pad, this is an indication that the offset is not equal to 0.5, in this case, the offset is 0.65. Additionally, the green dots indicate the pad center of curvature. The green dot is associated with the pad on the opposite side of the bearing, that is, the pad radius is larger than that of the journal, indicating a preload.

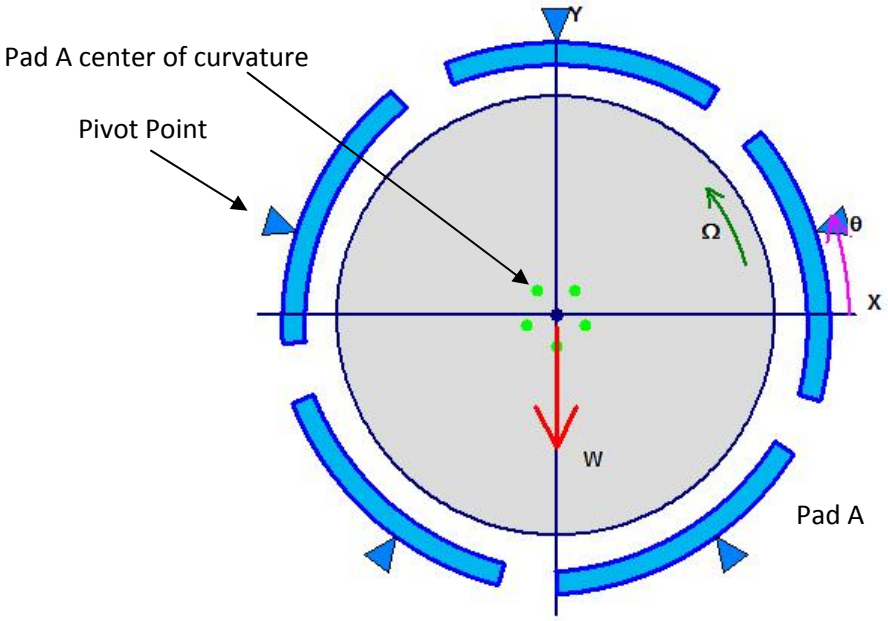

Figure 4.1: Tilting pad bearing nomenclature.

Tilting pad bearings are designed to allow pivot in various configurations. A ball and socket or spherical pivot, for example, allows for movement in three dimensions, while the cylindrical pivot acts as a rocker. The cylindrical design is appropriate for application on a turbocharger and will be analyzed later in this chapter. For the initial trials, the pad effects such as pad inertia and bending are considered to be effectively negligent, greatly simplifying the calculations. Later trials will incorporate a rigid pad, tilting on a cylindrical pivot. The rigid pad assumes that the pad itself does not deform when loaded; this assumption is typically considered acceptable for smaller bearings. Larger bearings tend to be more susceptible to deformation, affecting (typically negatively) the bearing's stiffness and damping values. Additionally, it is noted that the support structure necessary to accommodate the tilting pads will require slightly more volume than the floating ring bearing. It is not possible to determine the feasibility of installing tilting pad bearings in the existing turbocharger housing without additional information.

4.2 *Stability Analysis of the Generic Tilting Pad bearing*

Similar to that which was done in Chapter Three, the stability analysis was performed on the tilting pad bearing. Again, the mode with the lowest logarithmic decrement was chosen for illustration in the figures below; the same speeds were chosen for illustration as well. It was found that negative logarithmic decrement values were non-existent throughout the entire operating range of the rotor, shown in Figures 4.2 a-c.

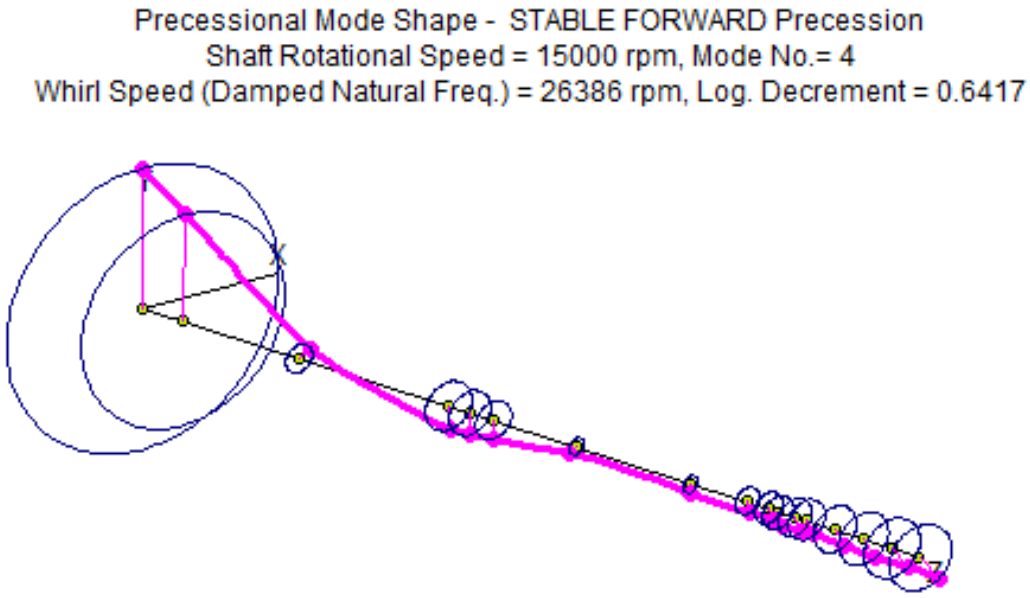

Figure 4.2a: Stable precession of rotor with tilting pad bearings at 15k rpm.

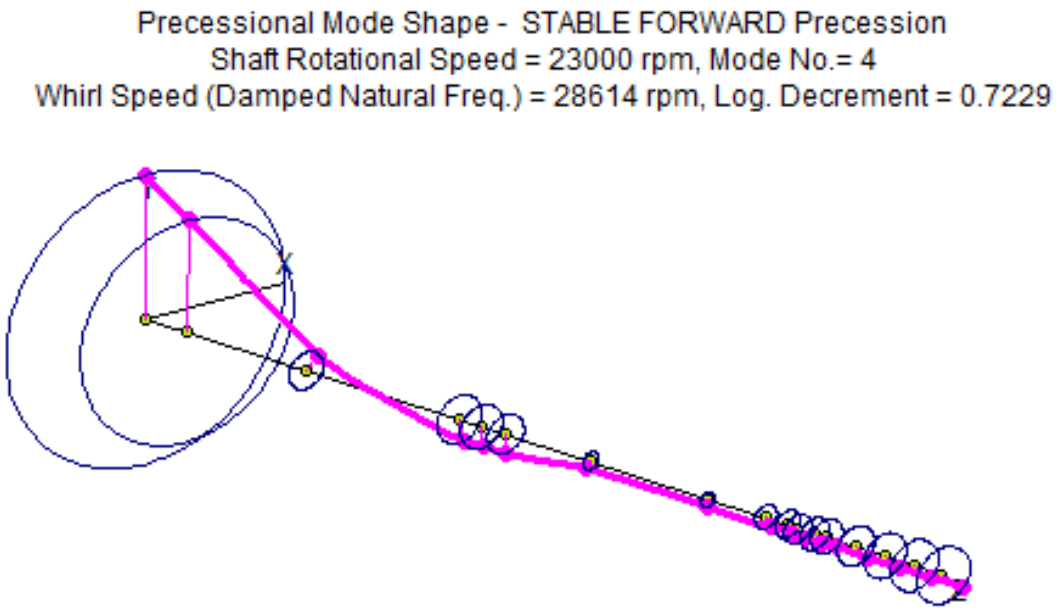

Figure 4.2b: Stable precession of rotor with tilting pad bearings at 23k rpm.

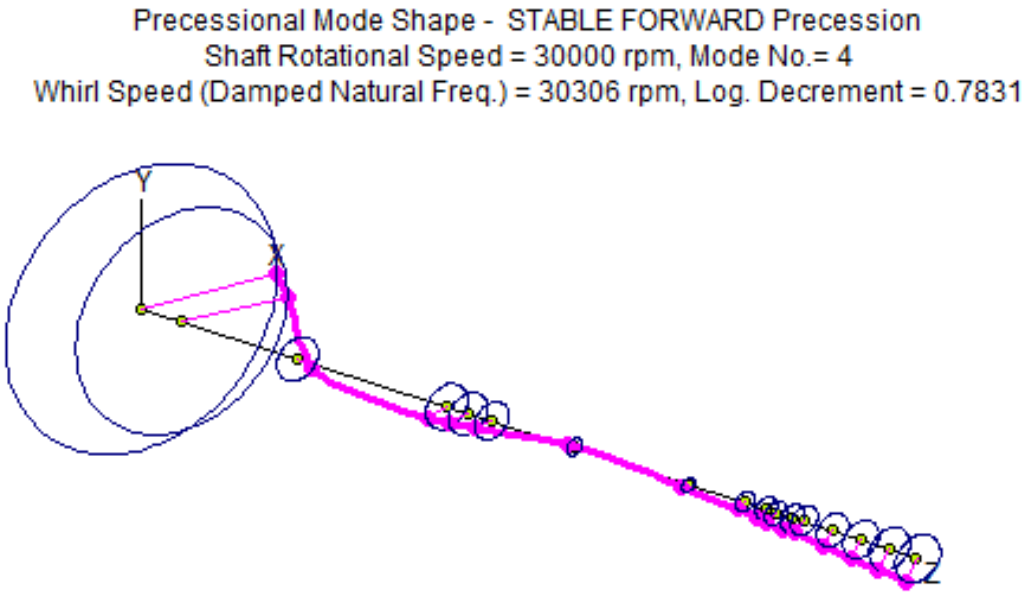

Figure 4.2c: Stable precession of rotor with tilting pad bearings at 30k rpm.

To ensure that no instabilities exist between the specific speeds chosen for analysis, the Stability Map was again created for a more continuous view of the logarithmic decrement over the entire operating range. Note that, unlike previous examples, the stability map remains positive throughout the designed speed range of the turbocharger. While the logarithmic decrement does become rather low at the higher speed values shown in Figure 4.3, the *designed* maximum speed is 30,000 rpm; only in an over speed situation would the rotor achieve speeds of 32,000 rpm, approaching unstable conditions.

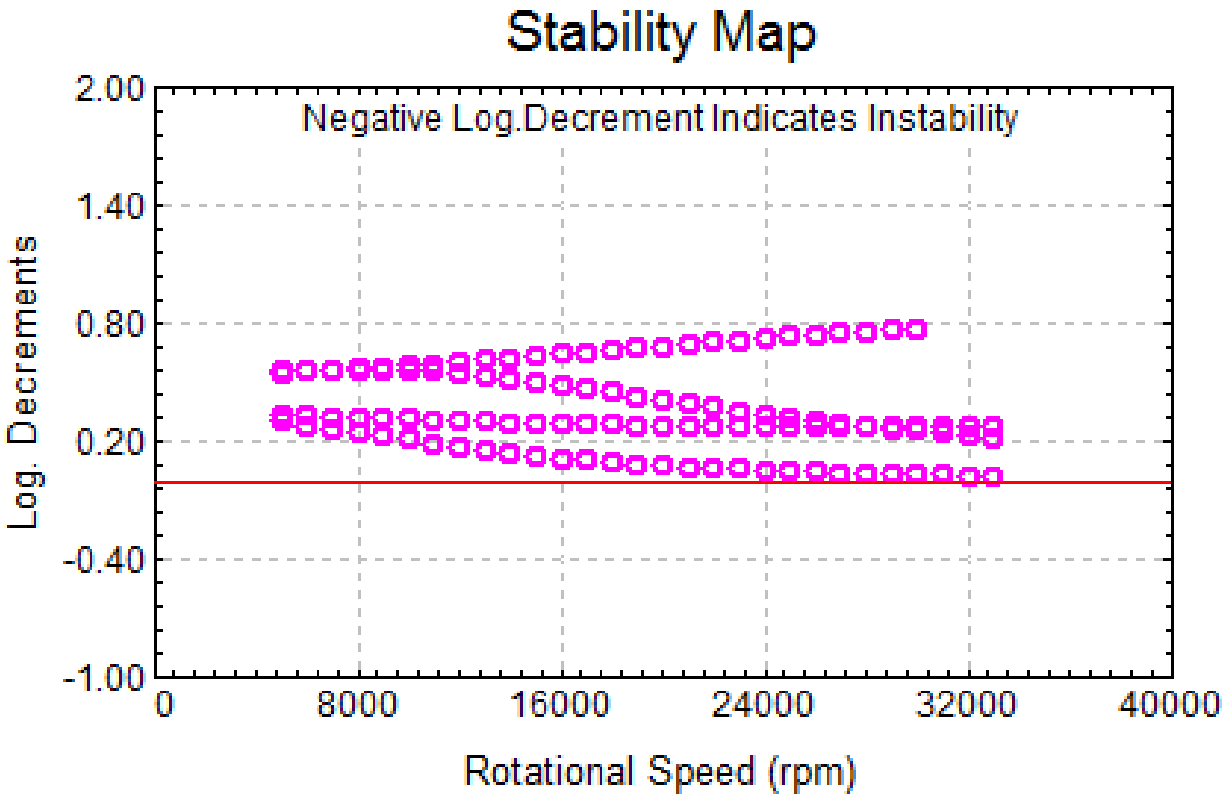

Figure 4.3: Stability map of rotor with tilting pad bearings.

In addition to the analysis of rotordynamic stability, it is obvious from previous examples that the displacement of the journal at the bearing locations is critical as well. As can be seen in

Figure 4.4, deflection at the compressor bearing is significantly reduced. The rotor maximum amplitude is just 0.2 mils from origin to peak amplitude, which produces no risk of bearing rub. The center of the plot is at zero rotational speed. The orbit grows as speed increases to 30k rpm, approaching a limit cycle, indicating minimal increased deflection even in over speed situations. This plot is shown in a different form in figure 4.5.

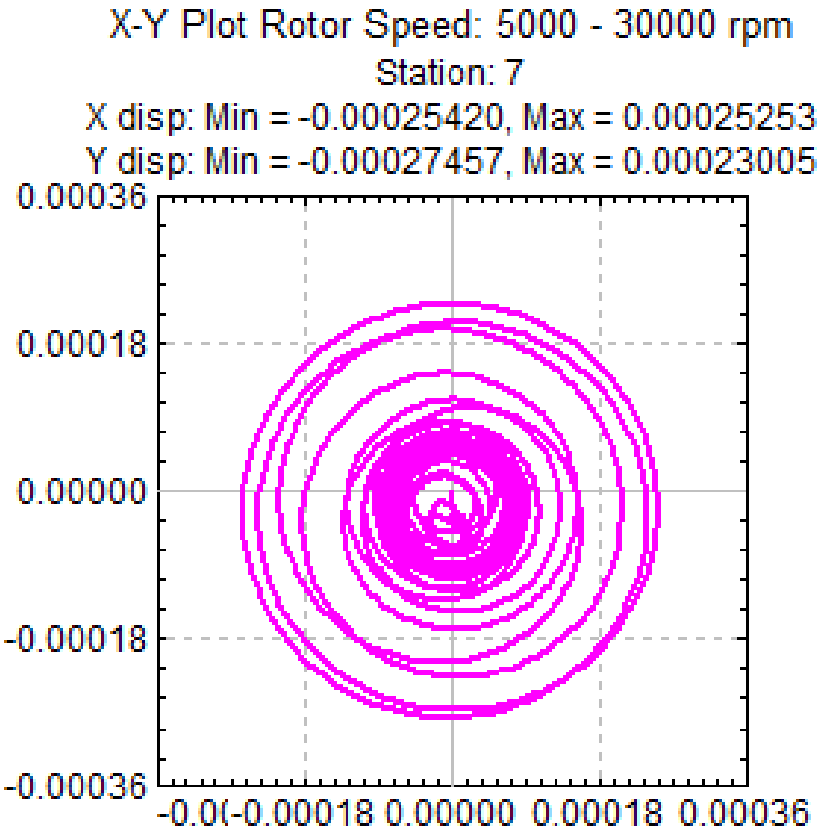

Figure 4.4: X-Y Orbit plot verses time of rotor with tilting pad bearings.

An easier to interpret plot can be seen in Figure 4.4, which portrays the X (red) and Y (pink) direction displacement as a function of rotor speed. This model provides a great visualization of the effects of critical speeds. A critical speed analysis of the rotor calculates critical speed

occurrences at 9k and 15k rpm, this is in agreement with the speeds at which increased deflection occurs in Figure 4.5.

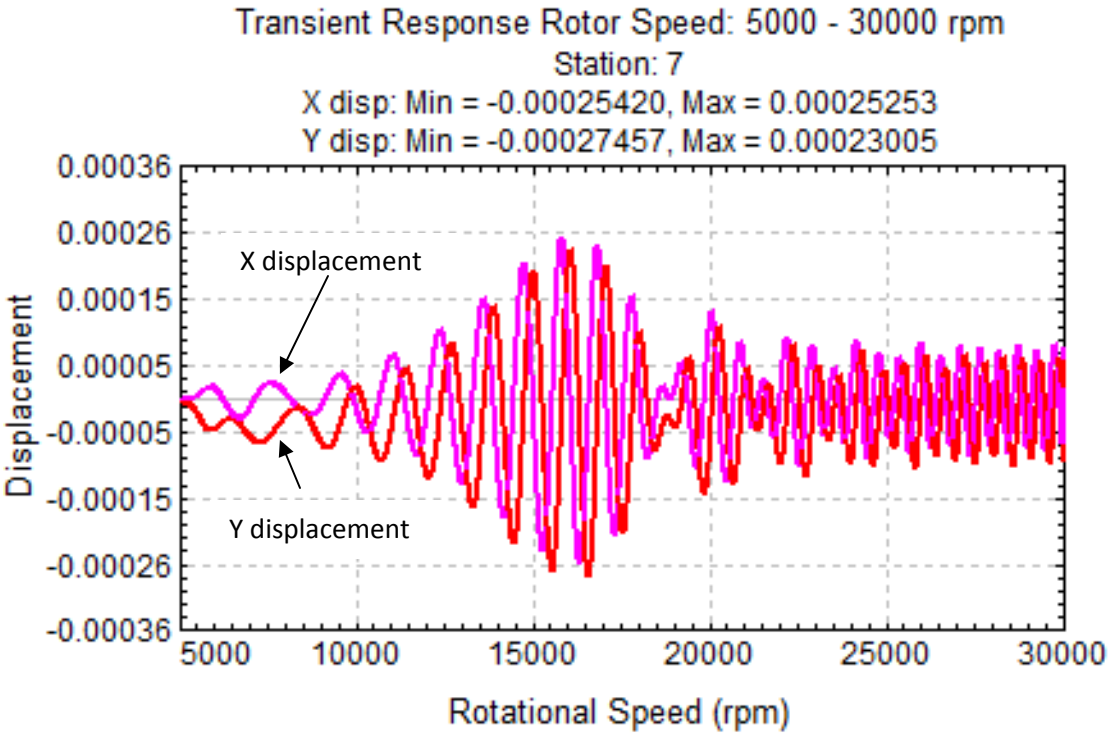

Figure 4.5: X (pink) and Y (red) deflection of rotor with tilting pad bearings vs rotor speed.

4.3 *Effects of Preload and Offset on Rotor-Bearing System Stability*

Stability analysis similar to section 4.2 will be presented with modified preload and offset values. To begin, the direct stiffness (pink) and damping(red) values for the standard offset(0.5) tilting pad bearing and offset (0.65) tilting pad bearing are compared. An offset value of 0.65 was chosen as this is commonly the higher end of normal offset values used in industry [9]. The stiffness and damping values are both similar, but noticeably higher for the offset bearing. It is apparent in Figures 4.6 a and b that the addition of offset very slightly increases the effective stiffness while slightly reducing the damping of the bearing.

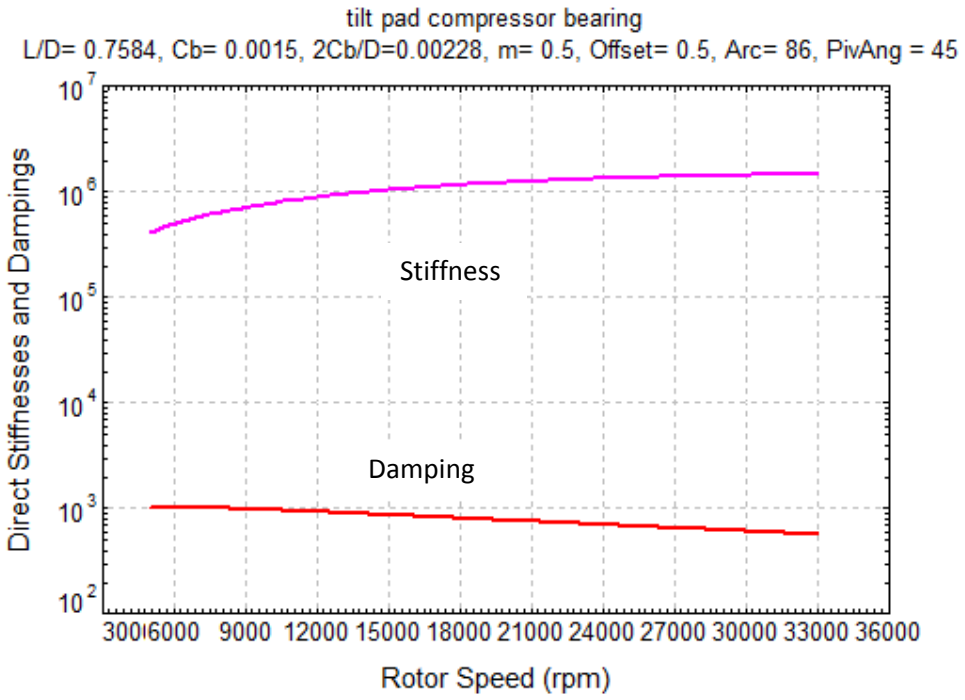

Figure 4.6a: Stiffness and damping of tilting pad bearing with offset 0.5.

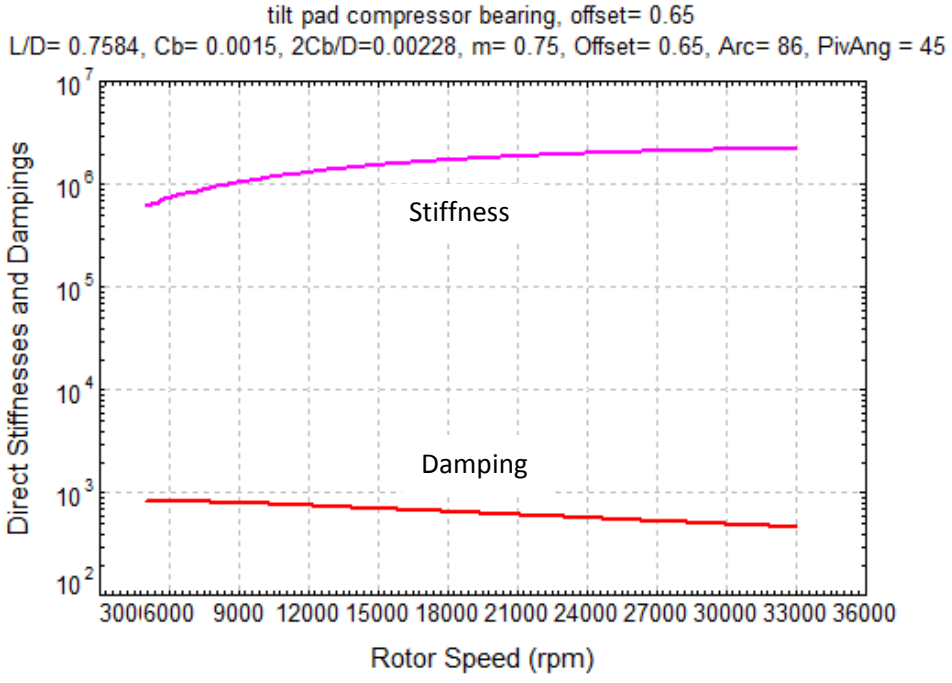

Figure 4.6b: Stiffness and damping of tilting pad bearing with offset 0.65.

While the change in bearing characteristics is minor in this case, it is still necessary to study the effects of these bearings on the rotor-bearing system. Figure 4.7 contains a Stability Map of the rotor system accounting for the offset bearing.

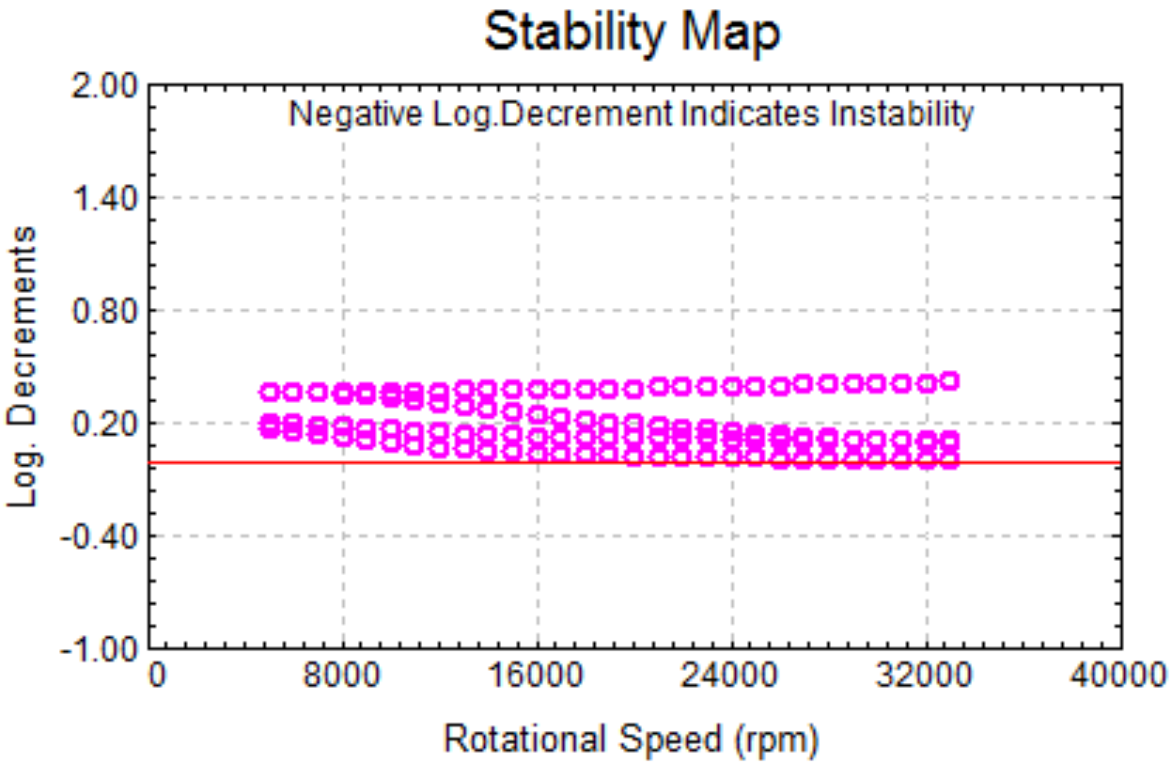

Figure 4.7: Stability Map of rotor with tilting pad bearings, offset = 0.65.

The Stability Map indicates a stable rotor system with minimal changes in logarithmic decrement compared to the tilting pad bearing with an offset value of 0.5. Figure 4.8 displays the deflection of the shaft at the bearing location as a function of speed.

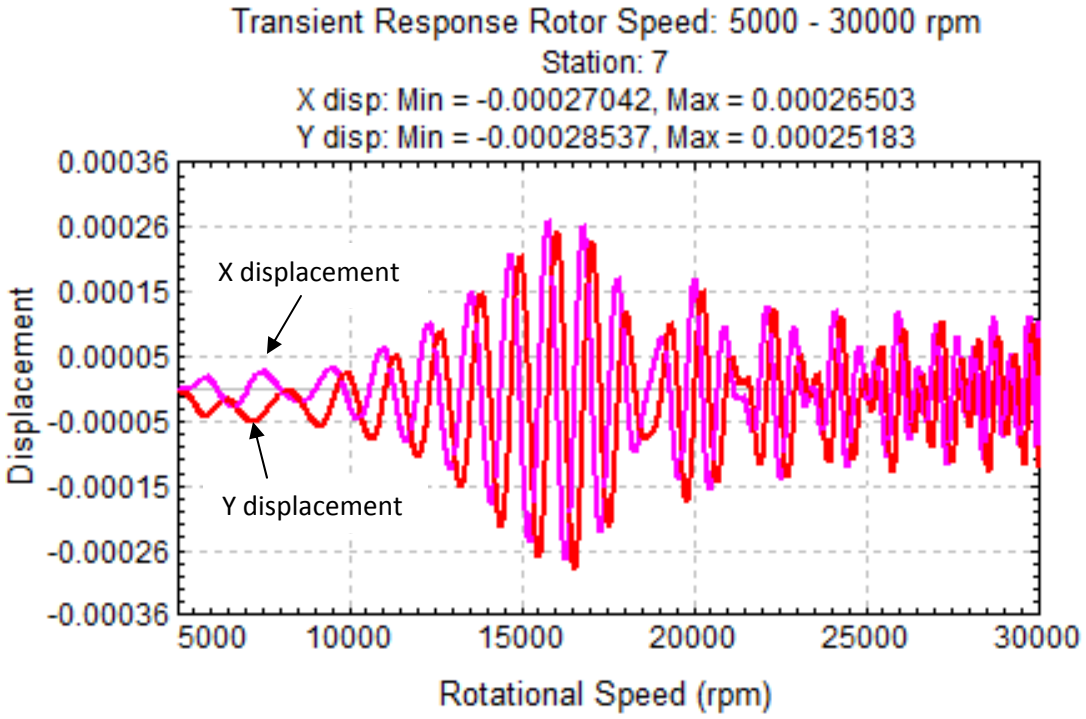

Figure 4.8: X (pink) and Y (red) deflection of rotor with tilting pad bearings vs rotor speed, offset = 0.65.

It is apparent that providing an offset to the installed bearing has a minimal effect on shaft stability and deflection. It is concluded that the extra machining involved in addition to the added risk of error during assembly is does not come at a significant advantage and is thus not warranted. The risk of error during assembly arrives with the offset causing the pad to not be symmetrical, introducing the possibility of installing the pad backwards.

4.4 *Tilting Pad Bearing with Pad Inertial Effects*

Finally, analysis will be conducted using the previously developed bearing (tilting pad, no offset, 0.5 preload) incorporating the inertial effects of the pads. Inertial effects are a very real part of tilting pad bearings, often dismissed as negligible in small bearings. These effects have been suspected to have mixed results on the stability of the rotor system; while the tilting pad conforms to the moving journal increasing stability, it is suspected to also permit oil whirl

causing cross-coupled instabilities similar to those in the plain or floating ring journal bearings [19]. This instability is often mitigated by using bearing preload. In Figure 4.9, it is apparent that the consideration of inertial effects has a slightly positive effect on the effective logarithmic decrement of the system.

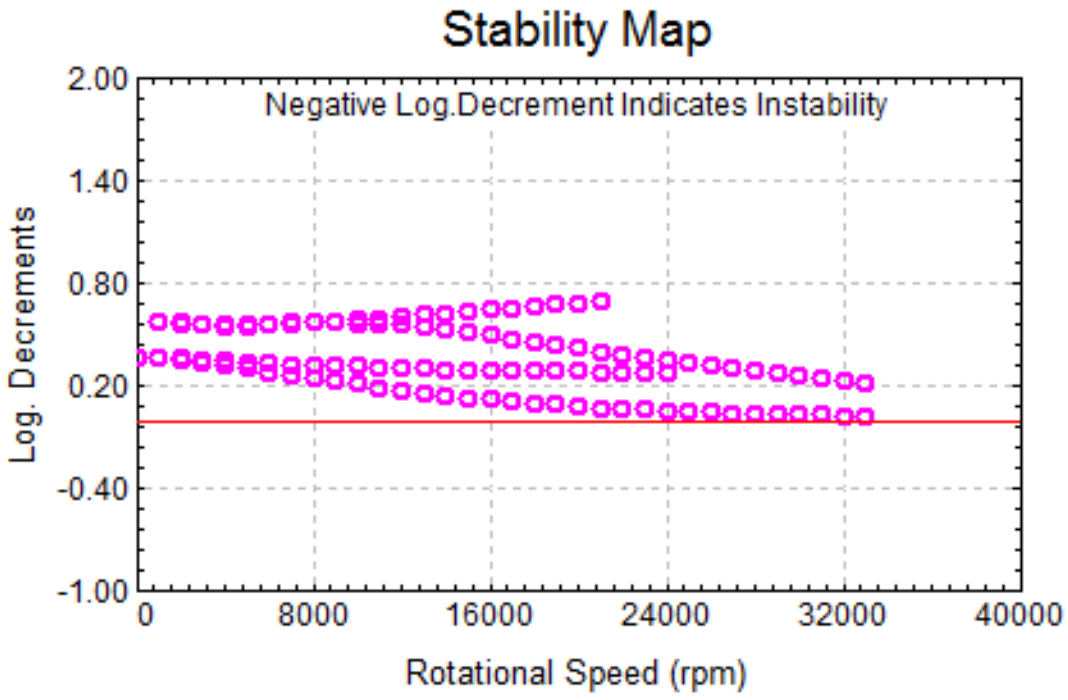

Figure 4.9: Stability Map of rotor with tilting pad bearings including inertial forces, offset = 0.5.

Figure 4.10 displays the calculated X and Y displacements of the shaft after considering pad inertial effects. It is apparent that there continues to be no risk of rubbing to the bearing due to vibration amplitudes.

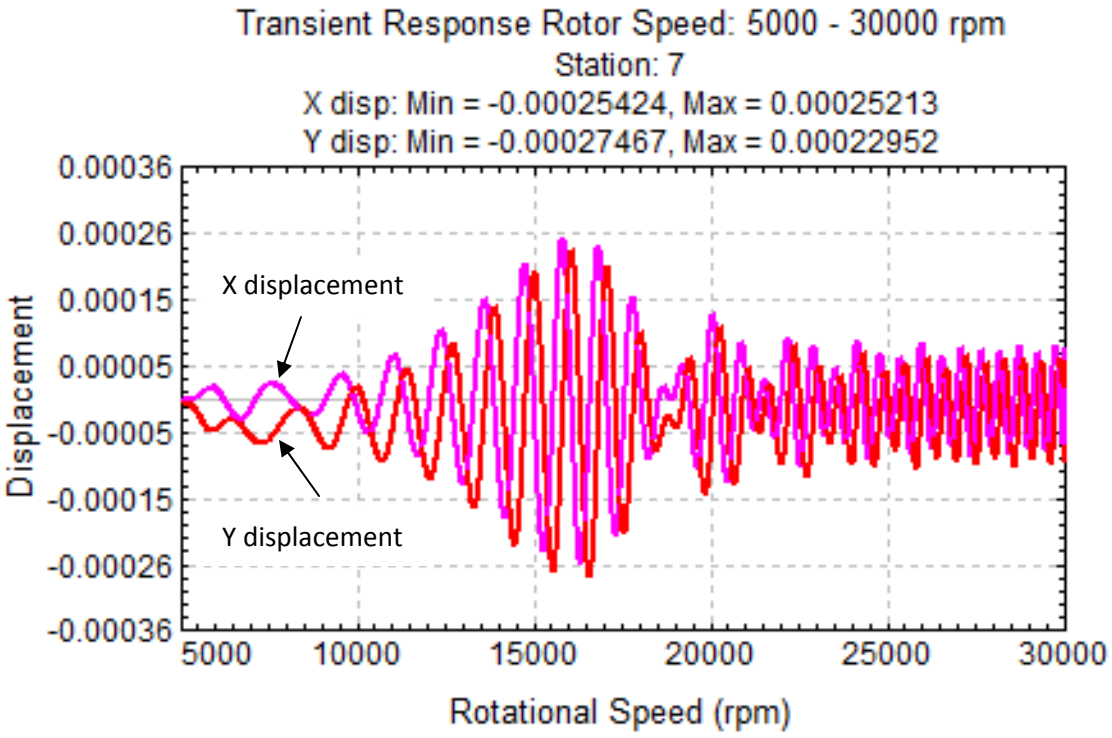

Figure 4.10: X (pink) and Y (red) deflection of rotor with tilting pad bearings vs rotor speed (with inertial effects).

After considering all aspects of the tilting pad bearing and all known turbocharger parameters, it is clear that the four pad tilting pad bearing with a 1.5 mil clearance, offset with a neutral value of 0.5, and a preload value of 0.5 will provided a more stable rotor-bearing system indicated by higher logarithmic decrement values and smaller vibration amplitudes. Experimental analysis is recommended using this design, and is strongly recommended for consideration analyzing application in a dynamic environment, discussed in section 5.2.

CHAPTER 5

CONCLUSIONS AND FUTURE STUDIES

5.1 *Conclusions*

Several bearings were introduced, along with a brief discussion of the strengths and shortcomings of each. Because actual units could not be obtained for measurement, bearing dimensions were assumed using industry standards, and a best case scenario to avoid falsely identifying unstable conditions. It was then introduced that several researchers have determined that limitations exist to the application of plain and floating ring journal bearings in high speed machinery such as turbochargers because oil whirl becomes severe enough to introduce instabilities. These limitations were confirmed analytically using rotordynamics software (DyRoBeS) to generate a model sharing similar rotordynamic properties as an actual turbocharger which has sustained failures while in service. Although DyRoBeS was not designed to analyze the hybrid "Floating Axial Groove" bearing, it was shown that the program's data could easily be modified to produce reasonable results. It became apparent that the bearings selected for use in the production version of this turbocharger, while inexpensive and commonly accepted for use in turbochargers in automotive applications, are not the proper bearings for this specialty application due to the cross-coupling forces introduced by the oil whirl in the fluid-films. The suspected mode of failure of the actual turbochargers, shaft shear due to seized bearings, was supported by the analytical findings from the software. Finally, after comparing several bearing options, an appropriate bearing design was modeled and shown to be stable over the entire operating range of the turbocharger. The stable bearing specifications are included in Table 5.1.

Table 5.1: Stable Bearing Characteristics

Bearing Type	4-pad Tilting Pad, load between pad
Clearance	0.0015 inches
Preload	0.5
Offset	0.5

Tables 5.2 and 5.3 contain samples of the overall data developed throughout the generation of this thesis. It is again apparent that the tilting pad bearing is the most stable bearing design included in this research. Table 5.2 contains the logarithmic decrement data for each bearing while Table 5.3 contains the peak amplitudes of vibration at designated speeds.

Table 5.2: Logarithmic Decrement Values for Various Bearings

Speed (rpm)	4 Axial Groove	Floating Axial Groove	Floating Ring	Tilting Pad
15,000	-0.52	1.79	-0.74	0.65
23,000	-0.42	-0.09	-1.49	0.72
30,000	-1.18	-0.56	-1.98	0.78

Table 5.3: Peak Amplitude of Vibration (origin to peak) of Various Bearings (mils)

Speed (rpm)	4 Axial Groove	Floating Axial Groove	Floating Ring	Tilting Pad
15,000	2.1	3.6	9.2	0.2
23,000	4.5	4.4	7.5	0.1
30,000	7.0	5.3	8.0	0.1

The operating environment of a buoy tender is typically in the vicinity of shoal water, and a replacement cost of a buoy tender is in excess of $40 million. With these considerations, along with the cost of the original turbocharger, the added cost of machining and materials shall not only be considered warranted, but in the overall situation shall be considered negligible.

5.2 *Future Studies*

This thesis has focused on the self-induced instabilities caused by fluid-film bearings and presented an alternative bearing which, if applied, would reduce shaft vibrations and extend the life of the selected turbocharger. Future studies focusing on the specific platform on which this turbocharger is mounted may shed light on additional sources of instability. The engine room of a ship, where the turbocharger of interest is located, contains multiple pieces of rotating machinery including various engines, reduction gears, compressors and pumps, fans, and propeller shafts- all of which induce various vibrations on adjacent machinery through foundations, hull plating, and structural support members.

Additionally, a study of thermal (Morton) effects is currently taking place at Virginia Tech, and will likely provide some additional factors contributing to the failure of this turbocharger. This study will also consider loadings on the compressor due to the pressurization and discharge of air to the serviced engine using the equations derived by Stepanoff [20].

Finally, gyroscopics due to the movement of the vessel has been discussed in limited detail in other literature as a potential failure method to shipboard turbochargers. The vessel served by this turbocharger is slightly over two-hundred feet in length, under 2,000 tons, and often operates in offshore environments. It is thus not uncommon for the vessel to encounter seas capable of causing moderate pitch and roll. Virginia Tech's Industrial Engineering

department has a test rig capable of reproducing this pitch and roll, and would be an ideal platform for testing the gyroscopic effects of a dynamic environment on a bearing-supported spinning rotor test rig.

REFERENCES

[1] ABMA, 2006, "Bearing Timeline."
[2] PRWeb, 2008, "Bearings market projected to reach $40 billion by 2010 ", http://www.prweb.com/releases/bearings/ball_roller_plain/prweb766124.htm.
[3] Chen, W. J., and Gunter, A. J., 2007, Introduction to Dynamics of Rotor-Bearing Systems, Trafford Publishing, Victoria, BC, Canada.
[4] Zeidan, F. Y., and Herbage, B. S., "Fluid Film Bearing Fundamentals and Failure Analysis," Proc. Proceedings of the Twentieth Turbomachinery Symposium, Texas A&M University.
[5] Watson, N., and Janota, M. S., 1982, Turbocharging the internal combustion engine, Wiley, New York.
[6] Alsaeed, A. A., 2005, "Dynamic Stability Evaluation of an Automotive Turbocharger Rotor-Bearing System," M.S., Virginia Tech, Blacksburg.
[7] Ehrich, F. F., 1999, Handbook of rotordynamics, Krieger Pub. Co., Malabar, FL.
[8] W. J. Chen, P. D., P.E., 2009, "DyRoBeS_Rotor," Eigen Technologies, Inc.
[9] W. J. Chen, P. D., P.E., 2009, "DyRoBes_BePerf," Eigen Technologies, Inc.
[10] Kirk, R. G., Alsaeed, A. A., and Gunter, E. J., 2007, "Stability Analysis of a High-Speed Automotive Turbocharger," Tribology transactions, 50(3), p. 427.
[11] Mondscehin, B. D., 2010, "Evaluation of Alternate Bearing Designs in a High Speed Automotive Turbocharger," M.S., Virginia Tech, Blacksburg.
[12] Kirk, R. G., and Edgar J. Gunter, J., 1970, "Transient Journal Bearing Analysis," University of Virginia, Charlottesville.
[13] Allaire, P. E., "INTRODUCTION TO JOURNAL BEARING DESIGN FOR TURBOMACHINERY," University of Virginia, Charlottesville.
[14] Budris, A. R., 2010, "Activated magnetic bearing potential for centrifugal pumps.(PUMP TIPS & TECHNIQUES)," Waterworld (Tulsa, Okla.), 26(3), p. 16.
[15] Crane, J., 2008, "Multilobe Specification sheet," http://www.johncrane.co.uk/Prod_ProdPage_Layout.asp?r=uk&l=en&ObjectItemID=9&element=Prod_ProdPage_BearingTech_1#.
[16] Andres, L. S., 2010, "MEEN 626: Modern Lubrication Theory," http://rotorlab.tamu.edu/me626/Notes_pdf/Modern%20Lub%20Notes%2001-15.pdf.
[17] Ltd., A. T. S., 2012, "ABB Turbocharging VTC Product Information," http://www05.abb.com/global/scot/scot208.nsf/veritydisplay/22769d0a786fbb06c12578ea003d7597/$file/abb%20turbocharging_vtc.pdf.
[18] Inc, T. T., 2010, "Table B.6 Room-Temperature Linear Coefficient of Thermal

Expansion Values for Various Engineering Materials," http://www.stormcable.com/uploads/Thermal_expansion_data_table_tb06.pdf.
[19] International Conference on Vibrations in Rotating, M., Institution of Mechanical Engineers . Tribology, G., Institution of Mechanical Engineers . Machine Systems, C., Control, G., and Rolls-Royce, L., "Self-excited vibration of rotors in tilting-pad journal bearings," Proc. Seventh International Conference on Vibrations in Rotating Machinery, 12-14 September 2000, University of Nottinham, UK, Professional Engineering Pub. for the Institution of Mechanical Engineers.
[20] Stepanoff, A. J., 1957, Centrifugal and axial flow pumps: theory, design, and application, Wiley, New York.